TÜBİTAK

Turkish Journal of Biology

http://journals.tubitak.gov.tr/biology/

Research Article

Turk J Biol
(2021) 45: 484-502

doi:10.3906/biy-2104-51

Determination of the interaction between the receptor binding domain of 2019-nCoV spike protein, TMPRSS2, cathepsin B and cathepsin L, and glycosidic and aglycon forms of some flavonols

Erman Salih İSTİFLİ[1], Arzuhan ŞIHOĞLU TEPE[2], Paulo A. NETZ[3], Cengiz SARIKÜRKCÜ[4], İbrahim Halil KILIÇ[5], Bektaş TEPE[6]

[1]Cukurova University, Faculty of Science and Literature, Department of Biology, Adana, Turkey
[2]Kilis 7 Aralık University, Vocational High School of Health Services, Department of Pharmacy Services, Kilis, Turkey
[3]Theoretical Chemistry Group, Institute of Chemistry, Universidade Federal do Rio Grande do Sul, Porto Alegre, Brazil
[4]Afyonkarahisar Health Sciences University, Faculty of Pharmacy, Department of Analytical Chemistry, Afyonkarahisar, Turkey
[5]Gaziantep University, Faculty of Science and Literature, Department of Biology, Gaziantep, Turkey
[6]Kilis 7 Aralik University, Faculty of Science and Literature, Department of Molecular Biology and Genetics, Kilis, Turkey

Received: 15.04.2021 • **Accepted/Published Online:** 05.06.2021 • **Final Version:** 30.08.2021

Abstract: The novel coronavirus (COVID-19, SARS-CoV-2) is a rapidly spreading disease with a high mortality. In this research, the interactions between specific flavonols and the 2019-nCoV receptor binding domain (RBD), transmembrane protease, serine 2 (TMPRSS2), and cathepsins (CatB and CatL) were analyzed. According to the relative binding capacity index (RBCI) calculated based on the free energy of binding and calculated inhibition constants, it was determined that robinin (ROB) and gossypetin (GOS) were the most effective flavonols on all targets. While the binding free energy of ROB with the spike glycoprotein RBD, TMPRSS2, CatB, and CatL were –5.02, –7.57, –10.10, and –6.11 kcal/mol, the values for GOS were –4.67, –5.24, –8.31, and –6.76, respectively. Furthermore, both compounds maintained their stability for at least 170 ns on respective targets in molecular dynamics simulations. The molecular mechanics Poisson–Boltzmann surface area (MM/PBSA) calculations also corroborated these data. Considering Lipinski's rule of five, ROB and GOS exhibited 3 (MW>500, N or O>10, NH or OH>5), and 1 (NH or OH>5) violations, respectively. Neither ROB nor GOS showed AMES toxicity or hepatotoxicity. The LD_{50} of these compounds in rats were 2.482 and 2.527 mol/kg, respectively. Therefore, we conclude that these compounds could be considered as alternative therapeutic agents in the treatment of COVID-19. However, the possible inhibitory effects of these compounds on cytochromes (CYPs) should be verified by in vitro or in vivo tests and their adverse effects on cellular energy metabolism should be minimized by performing molecular modifications if necessary.

Key words: 2019-nCoV, spike glycoprotein, TMPRSS2, CatB, CatL, flavonol, molecular docking, molecular dynamics, MM/PBSA

1. Introduction

Coronaviruses are positive sense RNA viruses with a diameter of 60–140 nm. As a result of electron microscopy studies, they were named as coronavirus since they carry spike proteins that cause a crown-like appearance on their surfaces (Richman et al., 2016). So far, four types of coronaviruses named as OC43, 229E, NL63, and HKU1 have been identified that circulate among humans. These pathogens usually cause mild respiratory infections in humans (Singhal, 2020).

In the past 20 years, two events have been recorded in which animal beta coronaviruses infected humans and caused serious consequences. In the first of these events, a beta coronavirus named as SARS-CoV passed from bats to humans via an intermediary host (palm civet cats) in the Guangdong province of China during the period of 2002–2003. SARS-CoV, which caused severe acute respiratory infection, affected 8422 people. However, the majority of the affected people lived in China and Hong Kong. The SARS-CoV epidemic caused 916 people to die (mortality rate 10.87%)(Chan-Yeung and Xu 2003). Approximately 10 years after this event, another beta coronavirus named as Middle East Respiratory Syndrome Coronavirus (MERS-CoV) appeared in Saudi Arabia. MERS-CoV has been transferred to humans using dromedary camels as the intermediate host. As a result of this epidemic, 2494 people were affected and 858 died (34.40% mortality rate) (Memish et al., 2020).

The third event in which another beta coronavirus caused an outbreak in humans occurred in Wuhan, China

* Correspondence: bektastepe@yahoo.com

in late December 2019. This virus, named 2019-nCoV by the World Health Organization (WHO), has been identified as an infectious agent of respiratory tract similar to the SARS virus in humans. Then, the genome sequence of the virus was determined by the Shanghai Public Health Clinical Center and it was suggested that the pathogen was of bat origin (Chan et al., 2020). The cases were reported to originate from the Huanan Seafood Wholesale Market (Huang et al., 2020). It was understood that 2019-nCoV could be transferred among people, with the infection transmitted from a patient, who was being treated in a hospital in Wuhan city, to 15 healthcare professionals in close contact (Wang et al., 2020). As of May 26, 2021, 2019-nCoV reached 168,867,700 cases from all over the world, causing the death of 3,506,342 people[1].

It is known that 2019-nCoV recruits the ACE2 receptor as the first gate in the process of entering the host cell. As a result of studies investigating the molecular interaction of the spike glycoprotein of the virus with the ACE2 receptor, it has been determined that leucine (455), phenylalanine (486), glutamine (493), serine (494), asparagine (501), and tyrosine (505) located in the receptor binding domain (RBD) of the spike protein play a primary role in the interaction (Zakaryan et al., 2017; Andersen et al., 2020). Following the binding of the RBD to the host cell receptor, the proteolytic cleavage of S protein at the S1/S2 interface and S2' sites with the help of transmembrane protease, serine 2 (TMPRSS2), and/or cathepsins B/L (CatB/L) allows access to the host cellular cytosol (Simmons et al., 2005;Kawase et al., 2012; Zhou et al., 2015; Shirato et al., 2017; Shirato et al., 2018; Iwata-Yoshikawa et al., 2019; Cannalire et al., 2020). These first steps that SARS-CoV-2 utilize in its entry into the host cell are a unique cascade that can be targeted in reducing or completely abolishing the viral capacity of the virus. This type of blockage can only be achieved by simultaneous inhibition of spike, TMPRSS2, CatB, and CatL proteins. In a previous molecular modelling study on the ability of flavonoid molecules to block SARS-CoV-2 infection, such an approach has been shown to be rational (Istifli et al., 2020).

Many researchers have revealed that phytochemicals (especially flavonoids) are excellent compounds with strong antiviral effects on colds, flu, and other infectious diseases. Besides Madagascar, India has also decided to promote the use of plant-based phytochemicals to combat of COVID-19 infection (del Barrio et al., 2011; Vazquez-Calvo et al., 2017; Cataneo et al., 2019; Chen et al., 2019; Chen et al., 2019; Dai et al., 2019; LeCher et al., 2019; Mohd et al., 2019; Nagai et al., 2019; Parvez et al., 2019; Sochocka et al., 2019; Trujillo-Correa et al., 2019; Dwivedi et al., 2020; Ling et al., 2020; Lopes et al., 2020; Ritta et al., 2020; Tang et al., 2020). Flavonoids constitute a large group of polyphenols found in plants. They are examined under different groups in terms of their chemical structure (flavonols, flavones, flavanones, flavanols, anthocyanidins, isoflavones, dihydroflavonols, and chalcones).

Flavonols are one of the most common flavonoids in nature. Phytochemicals in this group are abundant in both aglycon and glycosidic form in the foods we consume frequently. It is known that flavonols, which are abundant in vegetables and fruits, are also noteworthy in wine, tea, grape, apple, and onion. The vast majority of flavonols are derived from the simplest built member, 3-hydroxyflavone. The best known flavonol is quercetin and is abundant in plants. Fisetin, morin, tamarixetin, isorhamnetin, myricetin, and kaempferol are other common flavonols. Among them, myricetin and kaempferol are common in many foods. Tamarixetin and isorhamnetin are structurally methylated metabolites of quercetin. After the consumption of this compound, the amounts of these phytochemicals increase in tissues or plasma. Studies show that daily intake of flavonol is 20–35 mg/day and quercetin and glycosides constitute more than half of this rate. As with many other phytochemicals, the bioavailability rate of flavonols depends on the presence of additional bound structures, such as oligosaccharide units that affect their solubility. Thus, the glycosidic forms of flavonols are more effective biological/pharmacological agents than aglycon forms (Dávalos et al., 2006; Perez-Vizcaino and Duarte 2010).

In this study, as mentioned above, the molecular interaction of certain flavonols (in the forms of aglycon and glycosidic) (Figure 1), which is an important subgroup of flavonoids, with the RBD of 2019-nCoV, TMPRSS2, CatB, and CatL was investigated by computer-based molecular docking and molecular dynamics analyses. Based on the binding free energy (kcal/mol) and calculated inhibition constant (mM) values obtained from docking analysis, 'hit' flavonols were determined by calculating relative binding capacity index (RBCI) and further molecular dynamics and MM/PBSA analyses were performed on these phytochemicals.

2. Materials and methods

2.1. Ligand preparation

In this study, the 23 ligands (3-hydroxyflavone, azaleatin, galangin, gossypetin, kaempferide, natsudaidain, pachypodol, rhamnazin, amurensin, fisetin, astragalin, azalein, morin, hyperoside, icariin, rhamnetin, myricitrin, kaempferitrin, quercitrin, robinin, troxerutin, spiraeoside, and xanthorhamnin) with their protein data bank (pdb) file formats were retrieved from PubChem[2]. The geometry

[1]Outbreak C (2020). Coronavirus Outbreak [online]. Website https://www.worldometers.info/coronavirus/ [Accessed 24 April 2020]

[2]https://pubchem.ncbi.nlm.nih.gov

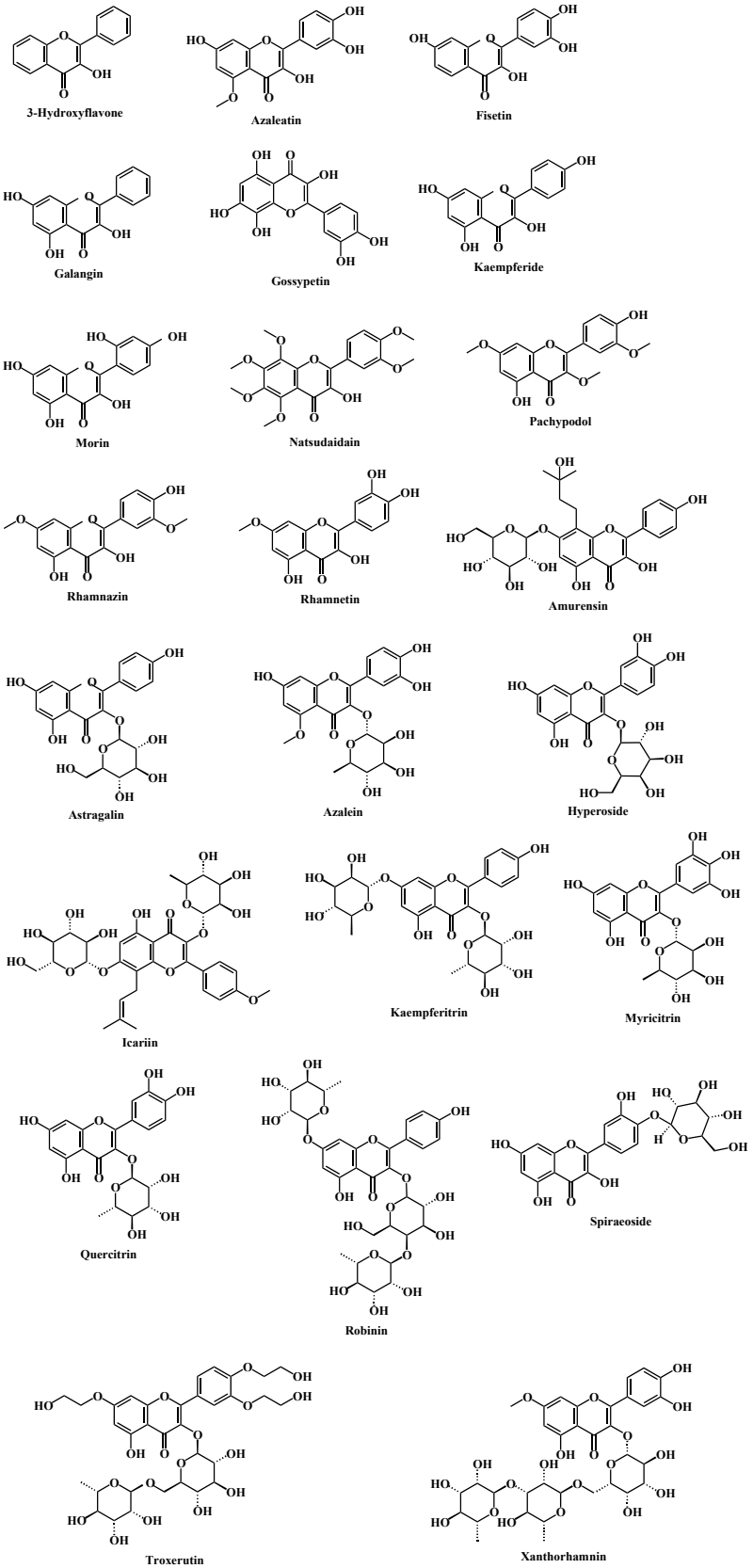

Figure 1. Chemical structures of the flavonols.

of the ligands were optimized using MMFF94 force field implemented in the Avogadro software.

2.2. Protein preparation using nanoscale molecular dynamics (NAMD)

Energy minimization of all receptor proteins (2019-nCoV ACE2-RBD, TMPRSS2, CatB, and CatL) were performed using NAMD according to the method given in the literature (Pedretti et al., 2004; Camacho et al., 2009; Remmert et al., 2012). Details were given in the supplementary file.

2.3. TMPRSS2 homology modeling

In line with the literature data regarding TMPRSS2 (Colovos and Yeates, 1993; Laskowski et al., 1993; Guex et al., 2009; Remmert et al., 2012; Studer et al., 2020), details on the process of generating the homology model were given in the supplementary file.

2.4. Molecular docking studies

Molecular docking studies were performed following the method given in the literature (Sanner, 1999; Greenspan et al., 2001; Wilson et al., 2005; Morris and Lim-Wilby 2008; Morris et al., 2009; Hardegger et al., 2011; Nasab et al., 2017; Andersen et al., 2020; Lan et al., 2020; Omotuyi et al., 2020; Wang et al., 2020; Woo et al., 2020; De Andrade et al., 2021) and details of the process were given in the supplementary file.

2.5. Calculation of the relative binding capacity index (RBCI)

Considering the activities of flavonols discussed in the present study against all four targets, RBCI analysis was carried out by following the method given in the literature in order to determine the "hit" compounds (Sharma, 1996; Istifli et al., 2020). Details of the applied RBCI method are given in the supplementary file.

2.6. Drug-likeness and ADMET prediction

The drug-likeness and ADMET profile of hit flavonols were determined according to the methods given in the literature (Delaney, 2004; Vistoli et al., 2008; Pires et al., 2015; Daina et al., 2017; Daina et al., 2019) and details were given in the supplementary file.

2.7. Molecular dynamics analyzes and molecular mechanics Poisson–Boltzmann surface area (MM/PBSA) calculations

Molecular dynamics and MM/PBSA analyzes were performed following the methods elsewhere (Parrinello and Rahman, 1981; Jorgensen et al., 1983; Hoover 1985; Darden et al., 1993; Essmann et al., 1995; Baker et al., 2001; Jakalian et al., 2002; Wang et al., 2004; Duan et al., 2009; O'Boyle et al., 2011; Homeyer and Gohlke 2012; Sousa da Silva and Vranken, 2012; Kumari et al., 2014; Abraham et al., 2015). Details of these molecular simulations were included in the supplementary file.

3. Results

The name of the flavonols, their PubChem CIDs, molecular weights, molecular formula, binding affinity (kcal/mol), and calculated inhibition constants (mM) along with their mean values and standard deviations (SD) were given in Table 1.

3.1. Molecular interaction of flavonols with the RBD of the spike glycoprotein

Detailed data on the nonbonded interactions of flavonols with the 2019-nCoV RBD was given in Table S2 (see the supplementary file). According to the data in the table, the Van der Waals contacts were the leading interactions in the receptor-ligand interplay. Conventional and nonconventional H bonds were also found to be effective in these interactions. Considering the heatmap given in Figure S3, the flavonols that interacted most intensely with the RBD of the spike glycoprotein were kaempferide, natsudaidain, astragalin, kaempferitrin, spiraeoside, and xanthorhamnin. While rhamnazin, astragalin, icariin, myricitrin, quercitrin, and robinin (ROB) interacted extensively with catalytic residues of the RBD of the spike glycoprotein (Tyr505, Asn501, Ser494, Gln493, and Leu455), no molecular interactions were detected with Phe486, another active amino acid residue. According to the data in Table 1, the flavonol that had the strongest interaction with spike glycoprotein was astragalin. The binding affinity and calculated inhibition constant of this compound were determined to be –6.35 kcal/mol and 0.022 mM, respectively.

3.2. Molecular interaction of flavonols with TMPRSS2

The molecular interaction of flavonols with TMPRSS2 was given in Table S3 in the supplementary file. Similar to the interaction of flavonols with spike glycoprotein, Van der Waals contacts were found to dominate the interactions of flavonols with TMPRSS2. Classical H bonds were also detected in the flavonol-TMPRSS2 interaction. According to the heatmap given in Figure S4, flavonols exhibiting the most intense interaction with TMPRSS2 were 3-hydroxyflavone, azaleatin, fisetin, galangin, gossypetin (GOS), rhamnetin, amurensin, astragalin, quercitrin, and spiraeoside. While flavonols showed a significant interaction with the active amino acid residues of TMPRSS2, His296 and Ser441, only 3-hydroxyflavone was found to interact with another active amino acid, Asp345. Flavonols with binding free energy greater than -5.0 kcal/mol were 3-hydroxyflavone, fisetin, ROB, and GOS (Table 1). On the other hand, binding free energies of icariin, kaempferitrin, troxerutin and xanthorhamnin were found to be unfavorable (positive).

In order to explain in more detail, the molecular interactions of ROB and GOS with TMPRSS2, the binding

Table 1. PubChem CID, molecular weight, molecular formula, free energy of binding and calculated inhibition constant values of the compounds.

No	Compound	PubChem CID	Molecular weight (g/mol)	Molecular formula	Free energy of binding (kcal/mol)				Calculated inhibition constant (mM)			
					Spike RBD	TMPRSS2	CatB	CatL	Spike RBD	TMPRSS2	CatB	CatL
1	3-Hydroxyflavone	11349	238.24	$C_{15}H_{10}O_3$	-5.61	-5.68	-6.96	-6.32	0.076	0.068	0.008	0.023
2	Azaleatin	5281604	316.26	$C_{16}H_{12}O_7$	-4.64	-4.39	-7.34	-5.93	0.398	0.610	0.007	0.044
3	Fisetin	5281614	286.24	$C_{15}H_{10}O_6$	-5.40	-5.13	-7.45	-6.29	0.109	0.172	0.003	0.024
4	Galangin	5281616	270.24	$C_{15}H_{10}O_5$	-5.45	-4.03	-6.43	-6.02	0.100	0.702	0.019	0.038
5	Gossypetin	5280647	318.23	$C_{15}H_{10}O_8$	-4.67	-5.24	-8.31	-6.76	0.380	0.144	0.0008	0.011
6	Kaempferide	5281666	300.26	$C_{16}H_{12}O_6$	-5.38	-4.24	-6.58	-6.55	0.113	0.779	0.014	0.015
7	Morin	5281670	302.23	$C_{15}H_{10}O_7$	-5.83	-4.74	-6.31	-6.18	0.053	0.335	0.023	0.029
8	Natsudaidain	3084605	418.40	$C_{21}H_{22}O_9$	-5.27	-2.48	-7.25	-5.27	0.138	15.31	0.004	0.136
9	Pachypodol	5281677	344.30	$C_{18}H_{16}O_7$	-5.80	-4.49	-7.21	-6.26	0.055	0.510	0.005	0.025
10	Rhamnazin	5320945	330.29	$C_{17}H_{14}O_7$	-5.76	-4.56	-7.22	-5.96	0.059	0.451	0.005	0.043
11	Rhamnetin	5281691	316.26	$C_{16}H_{12}O_7$	-4.94	-4.79	-7.49	-6.22	0.240	0.306	0.003	0.027
12	Amurensin	5318156	534.50	$C_{26}H_{30}O_{12}$	-3.53	-0.99	-7.81	-6.16	2.61	188.46	0.002	0.030
13	Astragalin	5282102	448.40	$C_{21}H_{20}O_{11}$	-6.35	-0.45	-8.51	-6.48	0.022	469.13	0.0005	0.017
14	Azalein	5321320	462.4 0	$C_{22}H_{22}O_{11}$	-4.33	-1.42	-6.6	-7.05	0.675	90.76	0.014	0.006
15	Hyperoside	5281643	464.40	$C_{21}H_{20}O_{12}$	-5.65	-1.98	-7.24	-5.93	0.071	35.49	0.005	0.044
16	Icariin	5318997	676.70	$C_{33}H_{40}O_{15}$	-3.43	+9.01	-7.05	-6.79	3.07	nd[1]	0.006	0.010
17	Kaempferitrin	5486199	578.50	$C_{27}H_{30}O_{14}$	-3.82	+1.85	-7.51	-7.49	1.58	nd[1]	0.003	0.003
18	Myricitrin	5281673	464.40	$C_{21}H_{20}O_{12}$	-3.89	-0.89	-7.69	-6.80	1.40	224.1	0.002	0.010
19	Quercitrin	5280459	448.40	$C_{21}H_{20}O_{11}$	-5.23	-1.74	-6.98	-6.96	0.145	0.531	0.007	0.007
20	Robinin	5281693	740.70	$C_{33}H_{40}O_{19}$	-5.02	-7.57	-10.10	-6.11	0.209	0.0028	0.00005	0.033
21	Spiraeoside	5320844	464.40	$C_{21}H_{20}O_{12}$	-3.19	-4.02	-6.39	-5.97	4.57	1.13	0.020	0.042
22	Troxerutin	5486699	742.70	$C_{33}H_{42}O_{19}$	+0.44	+47.31	-4.06	-2.77	nd[1]	nd[1]	1.06	9.36
23	Xanthorhamnin	5351495	770.70	$C_{34}H_{42}O_{20}$	-4.13	+18.67	-6.71	-5.99	0.941	nd[1]	0.012	0.040
	Mean				-4,65	0,35	-7,18	-6,19	0,773	57,17	0,05	0,44
	SD				1,41	11,65	1,07	0,88	1,200	122,89	0,22	1,95

[1]nd: not determined (calculated inhibition constant value could not be determined because the binding energy of the molecule is positive)

mode of these two ligands was compared with Nafamostat, a proved experimental inhibitor of TMPRSS2 (PDB ID: 7MEQ). Nafamostat formed conventional hydrogen bonds with Asp435, Ser436, Gly439, and Gly464 residues of TMPRSS2, and also participated in the formation of carbon-hydrogen bonds with Gln438 and Gly472 residues. Nafamostat has additionally established Van der Waals contacts with residues Cys437, Asp440, Thr459, Trp461, Gly462, Cys465, Ala466, Arg470, and Pro471 (Figure S7). ROB has established conventional hydrogen bonds with His279, Gln317, Lys340, and Gly439 residues of TMPRSS2, as well as pi-donor hydrogen bonds and pi-pi T-shaped hydrophobic contacts with His296 residue. The ROB has additionally formed an alkyl bond with the Lys340 residue. In addition, van der Waals contacts formed with Val278, Val280, Cys281, Gly282, Cys297, Glu299, Tyr337, Thr341, Lys342, Trp384, Gly385, Thr393, Asp440, Ser441, and Trp461 residues played an important role for the snug fit of ROB into the catalytic pocket of TMPRSS2.

GOS formed conventional hydrogen bonds with Asn433, Asp435, Asp440, and Cys465 residues of TMPRSS2, and also participated in the formation of hydrophobic contacts with Cys437 (pi-alkyl), Cys465 (amide pi-stacked), and Ala466 (pi-sigma) residues. GOS

has additionally established an electrostatic pi-cation interaction with Ala386. In addition, Van der Waals contacts formed with Gly259, Ile381, Gly385, Glu388, Glu389, Asn398, Ala400, Val434, Ser436, and Lys467 residues played an important role for the snug fit of GOS into the catalytic pocket of TMPRSS2. To summarize, ROB interacted with TMPRSS2, similar to Nafamostat, via residues Gly439 and Trp461. GOS, like Nafamostat, interacted with Asp435, Ser436, Cys437, Cys465, and Ala466 residues of TMPRSS2. The residue Asp440 was the amino acid commonly used by Nafamostat, ROB, and GOS in binding to TMPRSS2. Finally, ROB also formed chemical bonds with His296 and Ser441, which are the residues in the catalytic triad of TMPRSS2.

3.3. Molecular interaction of flavonols with CatB and CatL

Molecular interactions of flavonols with CatB and CatL were given in Tables S4 and S5 in the supplementary file. Van der Waals contacts and conventional H bonds are among the prominent nonbonded interactions in the molecular contacts of flavonols with cathepsins. While nonclassical H bonds, hydrophobic and electrostatic interactions stand out in the interaction of flavonols with CatB, mixed π/alkyl, electrostatic, lone pair/π-sulfur, Van der Waals interactions and classical H bonds were effective in interaction with CatL.

As can be seen from Figure S5 (supplementary file), where the flavonol-CatB interaction was visualized, flavonols interacted extensively with the active amino acid residues of CatB. It was determined that the majority of flavonols interacted extensively, especially with His111. The flavonols that interacted most with the active amino acid residues of CatB were as follows: 3-hydroxyflavone, azaleatin, fisetin, galangin, gossypetin, kaempferide, morin, natsudaidain, pachypodol, rhamnazin, rhamnetin, amurensin, astragalin, and kaempferitrin. Among the flavonols, the compound with the highest affinity for CatB was ROB with binding free energy of –10.10 kcal/mol and calculated inhibition constant value of 0.00005 mM.

Data on the interaction of flavonols with CatL was given in Figure S6 (supplementary file). According to data presented, flavonols interacted with the Cys25, Gly67, Gly68, Leu69, Met70, and Met161 active amino acid residues of CatL flavonols also interacted with Asp114, Ile115, and Lys117. The flavonol with the highest affinity for CatL was kaempferitrin. The free energy of binding and calculated inhibition constant of this compound were determined to be –7.49 kcal/mol and 0.003 mM, respectively.

3.4. Results of RBCI analyses (determination of 'hit' flavonols)

In this study, since the free energy of binding and calculated inhibition constants of the flavonols given in Table 1 against four different targets were calculated separately, RBCI analysis was applied to see how the affinity of flavonols on the respective targets were ranked when all targets were considered together. The ranking obtained using the RBCI analysis was given in Figure 2. The numerical values regarding this ranking were also presented in Table S1. As a result of the applied RBCI method, it was determined that the flavonols with the highest affinity to all target proteins were ROB and GOS. The RBCI coefficients of these compounds were determined as –0.64 and –0.43, respectively. Based on this finding, ROB and GOS were determined as 'hit' compounds. Due to page constraints, to be more reader friendly, instead of giving the top-ranked conformation of all flavonols, the top-ranked conformation for ROB and GOS is presented in Figures 3 and 4, respectively. Therefore, instead of performing molecular dynamics analysis of all compounds, the next part of the study was continued with ROB and GOS.

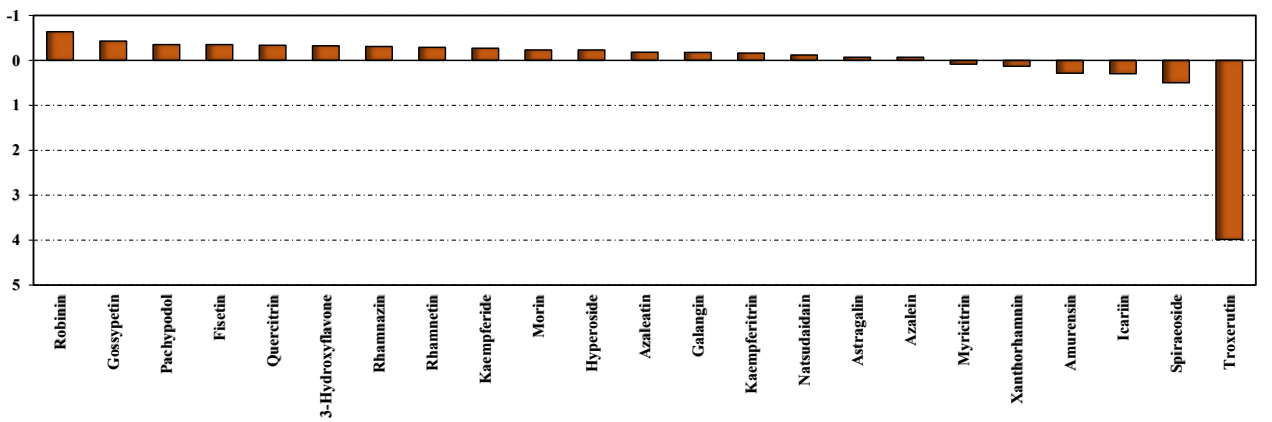

Figure 2. RBCI of the flavonols.

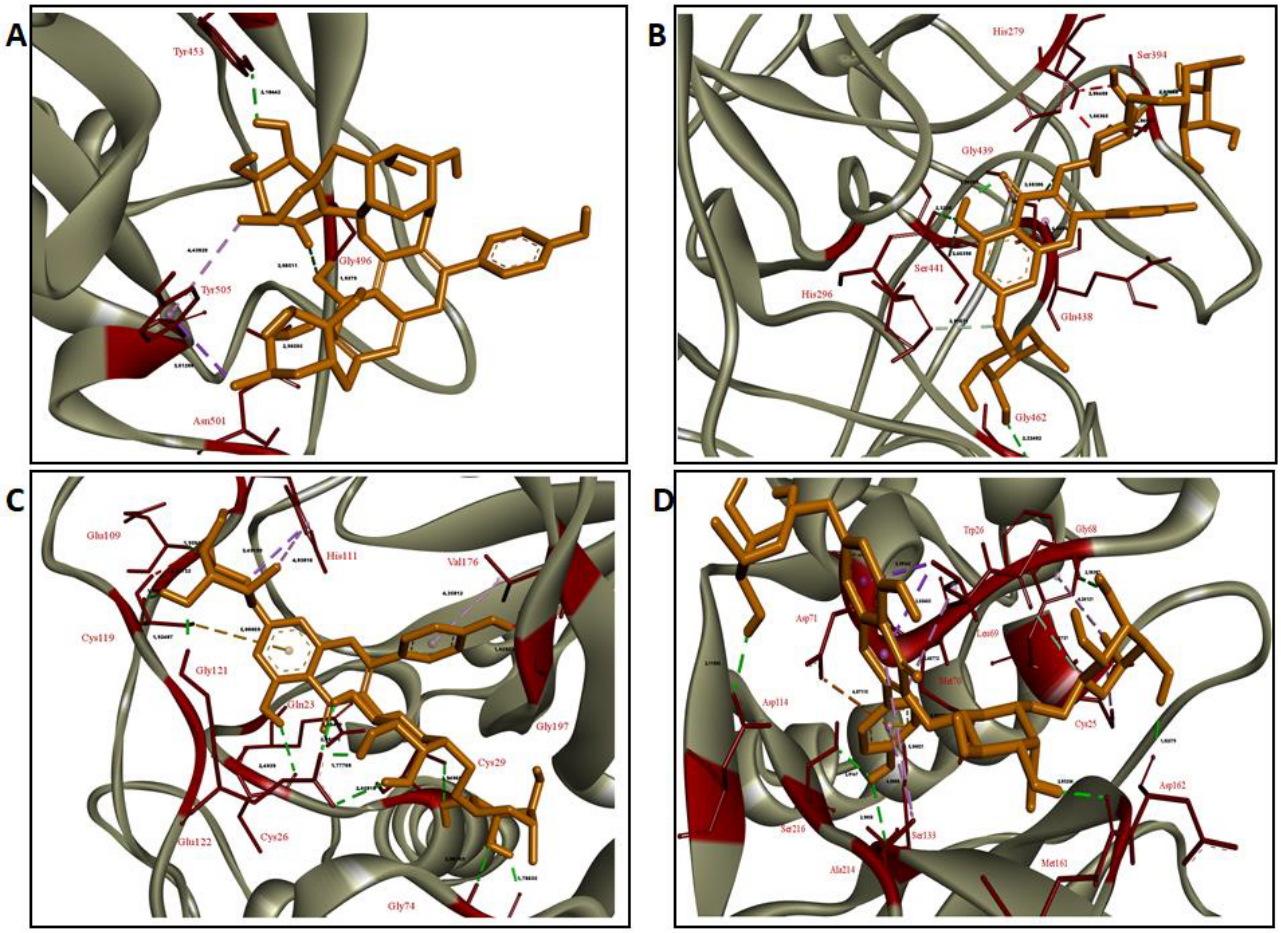

Figure 3. Top ranked conformations of robinin. (A- RBM of the spike glycoprotein of 2019-nCoV, BTMPRSS2, C- CatB, D- CatL).

3.5. Drug-likeness and ADMET predictions of the flavonols

The drug-likeness properties of flavonols were demonstrated in Table 2. According to Table 2, 3-hydroxyflavone, azaleatin, fisetin, galangin, kaempferide, morin, natsudaidain, pachypodol, rhamnazin, and rhamnetin did not show any violation. However, the 'hit' flavonols, GOS and ROB, exhibited 1 and 3 violations, respectively (GOS: NH or OH> 5 and ROB: NH or OH> 5, N or O> 10, MW> 500).

ADMET of flavonols were shown in Table 3. Based on the data in Table 3, none of the flavonols, except 3-hydroxyflavone, were able to pass the blood-brain barrier (BBB). It was understood that not all flavonols were substrate of P-gp, except for amurensin, icariin, and ROB. Since almost half of flavonols have an inhibitory effect on CYPs, it was thought that they may adversely affect the energy metabolism of the cell. None of the flavonols showed neither AMES toxicity nor hepatotoxicity. The LD_{50} values of the 'hit' flavonols, ROB and GOS, in rats were determined as 2.482 and 2.527 mol/kg, respectively.

3.6. Molecular dynamic analyses and binding free energy (MM/PBSA) calculations of 'hit' flavonoids

The ROB molecule, initially interacted with the residues Tyr453, Tyr489, Phe490, Tyr495, Gly496, Asn501, and Tyr505 of spike's RBM (Figure 5A). It remained interacting with the same residues until 77 ns, when the interaction with residues Tyr495, Gly496, and Tyr505 was lost and replaced with the interaction with the residues Phe456, Gly485, and eventually with Ala475. At 170 ns, a rearrangement took place and the ROB molecule interacted with the side loop (residues 475 until 479), remaining in this configuration until the end of the simulation. By the analysis of the trajectory and number of hydrogen bonds we can conclude that the interaction was moderately strong (Figure 5A).

The ROB molecule started interacting with the residues His279, Glu389, Val280, Lys390, Gly391, Lys392, Thr393, Gln438, Cys437, Gly439, Ser441, Asp440, and Ser463 of TMPRSS2 (Figure 5B). At 40 ns it started to interact also with Ser318 and Met320. At about 65 ns the ROB molecule underwent a conformational change and lost the contacts with the loop of the residues 389–393, but started to

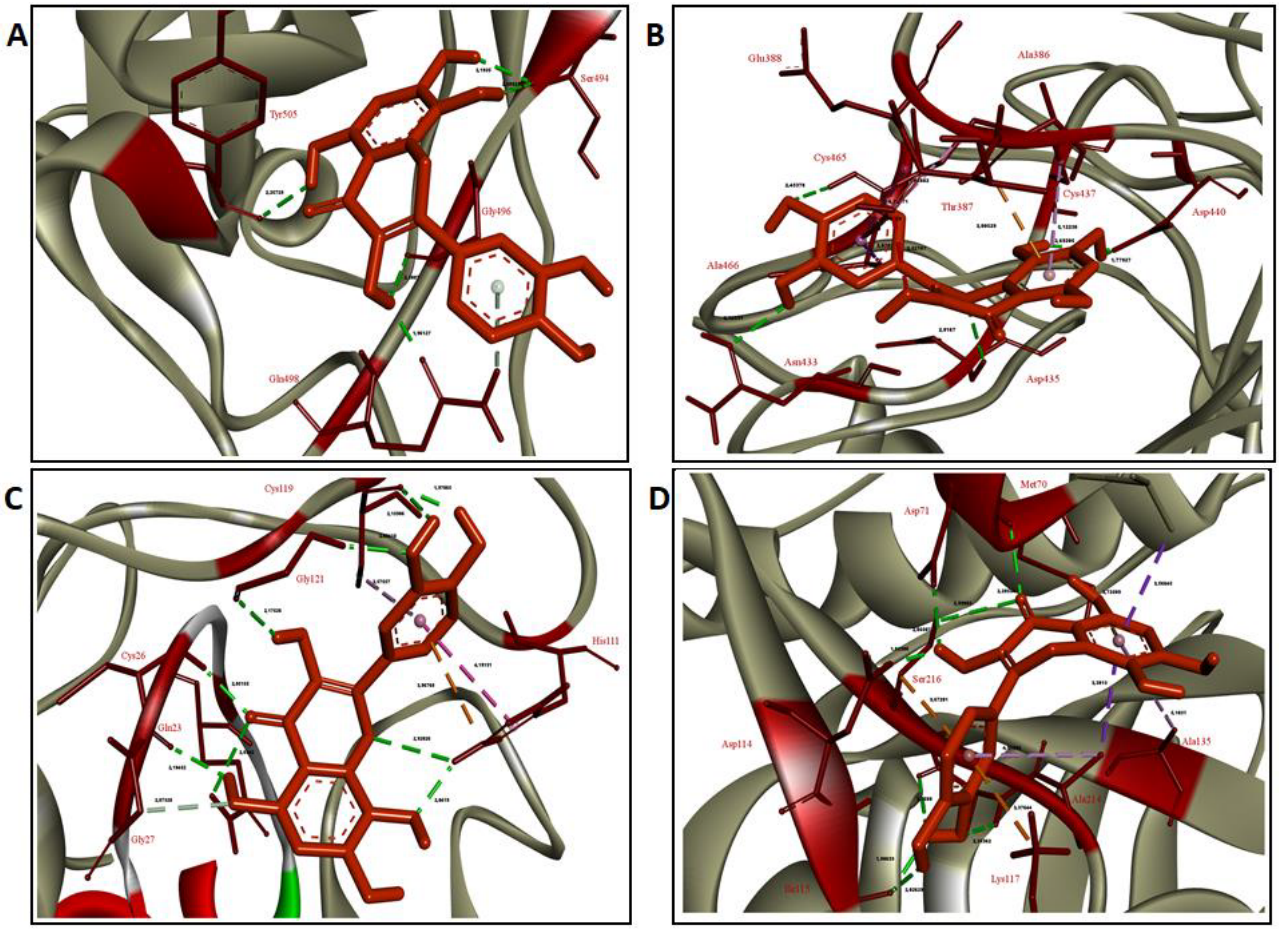

Figure 4. Top ranked conformations of gossypetin. (A- RBM of the spike glycoprotein of 2019-nCoV, B- TMPRSS2, C- CatB, D- CatL).

interact with His296, Lys340, Thr341, Lys342, Trp461, and Gly462. This conformation remained stable until the end of the simulation period. Analyzing the trajectory and the evolution of the hydrogen bond pattern let us to conclude that the interaction was strong (Figure 5B).

The ROB molecule started interacting with several residues of CatB: Ser25, Gln23, Gly27, Cys26, Cys29, Gly73, Gly74, Glu109, His111, His110, Val112, Pro118, Cys119, Gly121, Thr120, Glu122, Val176, Gly197, and Gly198 (Figure 5C). The interaction was very strong (with several hydrogen bonds) and, besides some rearrangement of external loops in CatB, the complex remained very stable. In the end of the simulation the interaction pattern is essentially the same, only the interactions with Gly121 and Glu122 were lost. By the analysis of the trajectory and the evolution of the hydrogen bond pattern we can conclude that the interaction was very strong (Figure 5C).

The ROB molecule started interacting with several residues CatL: Cys25, Trp26, Gly67, Gly68, Leu69, Met70, Asp71, Ser133, Val134, Asp160, Met161, Asp162, His163, Gly164, Ala214, and Ser216 (Figure 5D). At about 20 ns the ROB molecule suffered a reorientation and started to interact with Glu63, Asn66 and Gly159, losing the interactions with the residues 134 and 162–164. At about 85 ns the Cat-L molecule underwent a conformational transition in an outer loop with a short helix, not interacting with the ROB molecule. The pattern of interactions is essentially maintained throughout the simulation. In this case, again, by the analysis of the trajectory and the evolution of the hydrogen bond pattern we can conclude that the interaction was very strong (Figure 5D).

The interaction of GOS, our second top-ranked ligand, with spike's RBM is shown in Figure 6A. The GOS molecule started interacting with the residues Ser494, Tyr495, Gly496, Phe497, Gln498, and Tyr505. In a few nanoseconds, it migrated to the opposite edge of spike's RBM, interacting with Glu484, Gly485, Phe486, Asn487, Cys488, and Tyr489, where it remains until 80 ns, interacting eventually with Gln493 and Thr470. It detached briefly at 81 ns, returns to interact with the RBM and starting at 90 ns, until the end of the simulation, it interacted with the outer edge of the loop containing the

Table 2. Drug-likeness properties of docked flavonols.

No	Compound	Number of rotatable bonds	TPSA[1]	Consensus Log P	Log S (ESOL[2])	Drug-likeness (Lipinski's rule of five)
1	3-Hydroxyflavone	1	50.44	2.84	-4.05	Yes; 0 violation
2	Azaleatin	2	120.36	1.41	-3.02	Yes; 0 violation
3	Fisetin	1	111.13	1.55	-3.35	Yes; 0 violation
4	Galangin	1	90.90	1.99	-3.46	Yes; 0 violation
5	Gossypetin	1	151.59	0.96	-3.40	Yes; 1 violation: NH or OH>5
6	Kaempferide	2	100.13	2.00	-3.51	Yes; 0 violation
7	Morin	1	131.36	1.20	-3.16	Yes; 0 violation
8	Natsudaidain	7	105.82	2.71	-4.17	Yes; 0 violation
9	Pachypodol	4	98.36	2.61	-4.46	Yes; 0 violation
10	Rhamnazin	3	109.36	2.02	-3.56	Yes; 0 violation
11	Rhamnetin	2	120.36	1.63	-3.36	Yes; 0 violation
12	Amurensin	7	210.51	0.44	-3.61	No; 3 violations: MW>500, N or O>10, NH or OH>5
13	Astragalin	4	190.28	-0.25	-3.18	No; 2 violations: N or O>10, NH or OH>5
14	Azalein	4	179.28	0.51	-3.20	No; 2 violations: N or O>10, NH or OH>5
15	Hyperoside	4	210.51	-0.25	-3.04	No; 2 violations: N or O>10, NH or OH>5
16	Icariin	9	238.20	0.84	-4.73	No; 3 violations: MW>500, N or O>10, NH or OH>5
17	Kaempferitrin	5	228.97	-0.46	-3.33	No; 3 violations: MW>500, N or O>10, NH or OH>5
18	Myricitrin	3	210.51	-0.23	-3.20	No; 2 violations: N or O>10, NH or OH>5
19	Quercitrin	3	190.28	0.16	-3.33	No; 2 violations: N or O>10, NH or OH>5
20	Robinin	8	308.12	-1.82	-3.33	No; 3 violations: MW>500, N or O>10, NH or OH>5
21	Spiraeoside	4	210.51	-0.19	-3.64	No; 2 violations: N or O>10, NH or OH>5
22	Troxerutin	15	297.12	-1.36	-2.79	No; 3 violations: MW>500, N or O>10, NH or OH>5
23	Xanthorhamnin	9	317.35	-1.90	-3.55	No; 3 violations: MW>500, N or O>10, NH or OH>5

[1]TPSA: Topological polar surface area (Å^2)
[2]ESOL: Estimated aqueous solubility [(Insoluble < -10 < Poorly < -6 < Moderately < -4 < Soluble < -2 Very < 0 < Highly), according to Delaney, J.S. (2004)].
Data source: http://www.swissadme.ch/index.php#

residues 439 until 445, as well as with Pro499 and Thr500. The molecule probably migrated from a region with weak interactions to a region with moderate interactions (Figure 6A).

The GOS molecule started interacting with the residues Ser382, Ala386, Thr387, Glu388, Glu389, Ala399, Asn433, Val434, Asp435, Ser436, Cys437, Cys465, and Ala466 of TMPRSS2 (Figure 6B). Suffering only some small rearrangements, the molecule remained interacting essentially in the same place during all the simulation, losing only the interactions with Glu388, Glu389, and Asn433. Despite the low number of hydrogen bonds, considering the residence of the ligand in the protein pocket, the interaction is expected to be moderately strong to strong (Figure 6B).

The GOS molecule initially formed interactions with the residues Gln23, Gly24, Ser25, Cys26, Gly27, His110, His111, Cys119, Thr120, Gly121, Glu122, Leu181, and Gly197 of CatB (Figure 6C). It remained essentially in the same region in the protein, making eventually additional interactions with the residues Cys29 and Met196 and in the end of the simulation also with Trp221 and Asn222. Even considering that the hydrogen bond interactions are not much high in number, the high residence time of the ligand in the protein pocket let us conclude that the interaction is expected to be strong (Figure 6C).

The GOS molecule started interacting with the residues Gly68, Leu69, Met70, Asp71, Asp114, Lys117, Ala135, Asp160, Met161, Asp162, His163, Ala214, Ala215, and Ser216 of CatL (Figure 6D). It remained in

Table 3. ADMET profiles of flavonols.

No	Compound	BBB1 permeation[1,*]	P-gp substrate[2,*]	CYP inhibition[3,*]	AMES Toxicity[4]	Hepatotoxicity[4]	LD50 in rat (mol/kg)[4]
1	3-Hydroxyflavone	Yes	No	Yes (CYP1A2, CYP2C19, CYP2D6, CYP3A4)	Yes	No	1.991
2	Azaleatin	No	No	Yes (CYP1A2, CYP2D6, CYP3A4)	No	No	2.393
3	Fisetin	No	No	Yes (CYP1A2, CYP2D6, CYP3A4)	No	No	2.465
4	Galangin	No	No	Yes (CYP1A2, CYP2D6, CYP3A4)	No	No	2.450
5	Gossypetin	No	No	Yes (CYP1A2, CYP2D6, CYP3A4)	No	No	2.527
6	Kaempferide	No	No	Yes (CYP1A2, CYP2D6, CYP3A4)	No	No	2.338
7	Morin	No	No	Yes (CYP1A2, CYP2D6, CYP3A4)	No	No	2.413
8	Natsudaidain	No	No	Yes (CYP2C19, CYP3A4)	No	No	2.379
9	Pachypodol	No	No	Yes (CYP1A2, CYP2C9, CYP2D6, CYP3A4)	No	No	2.212
10	Rhamnazin	No	No	Yes (CYP1A2, CYP2C9, CYP2D6, CYP3A4)	No	No	2.241
11	Rhamnetin	No	No	Yes (CYP1A2, CYP2D6, CYP3A4)	No	No	2.453
12	Amurensin	No	Yes	No	No	No	2.634
13	Astragalin	No	No	No	No	No	2.546
14	Azalein	No	No	Yes (CYP3A4)	No	No	2.537
15	Hyperoside	No	No	No	No	No	2.541
16	Icariin	No	Yes	No	No	No	2.631
17	Kaempferitrin	No	Yes	No	No	No	2.587
18	Myricitrin	No	No	No	No	No	2.537
19	Quercitrin	No	No	No	No	No	2.586
20	Robinin	No	Yes	No	No	No	2.482
21	Spiraeoside	No	Yes	No	No	No	2.559
22	Troxerutin	No	Yes	No	No	No	2.476
23	Xanthorhamnin	No	Yes	No	No	No	2.477

[1]BBB: Blood Brain Barrier
[2]P-gp: P-glycoprotein substrate
[3]CYP: Cytochrome P
[4]http://biosig.unimelb.edu.au/pkcsm/prediction
[5]https://www.swissadme.ch

essentially the same position, but suffering some structural rearrangement, eventually interacting with the residue TRP26. In the end of the simulation, the contacts with the residues Asp114, Lys117, Ala214, Ala215, and Ser216 were lost and new contacts were made with Asn66 and Gly67. Even considering that the hydrogen bond interactions are not much high in number, the high residence time of the ligand in the protein pocket let us conclude that the interaction is expected to be strong (Figure 6D).

The RMSD of the ligands show that their structure shave converged in all simulations and remained stable, apart from some structural fluctuations related to torsional conformational transitions, yielding multiple similar conformations (in the case of ROB) and two conformations (in the case of GOS). The conformational transitions of the ligands, however, do not disturb the strong interactions with the receptors (Figures 5–6).

In the present, the binding free energy of the complexes formed by ROB and GOS with four different receptors was calculated by the MM/PBSA method. Both MM/PBSA and MM/GBSA are computational methods used to estimate the free energy of binding of small molecules to receptors (proteins, nucleic acids or other macromolecules) (Genheden and Ryde, 2015). In both methods the free

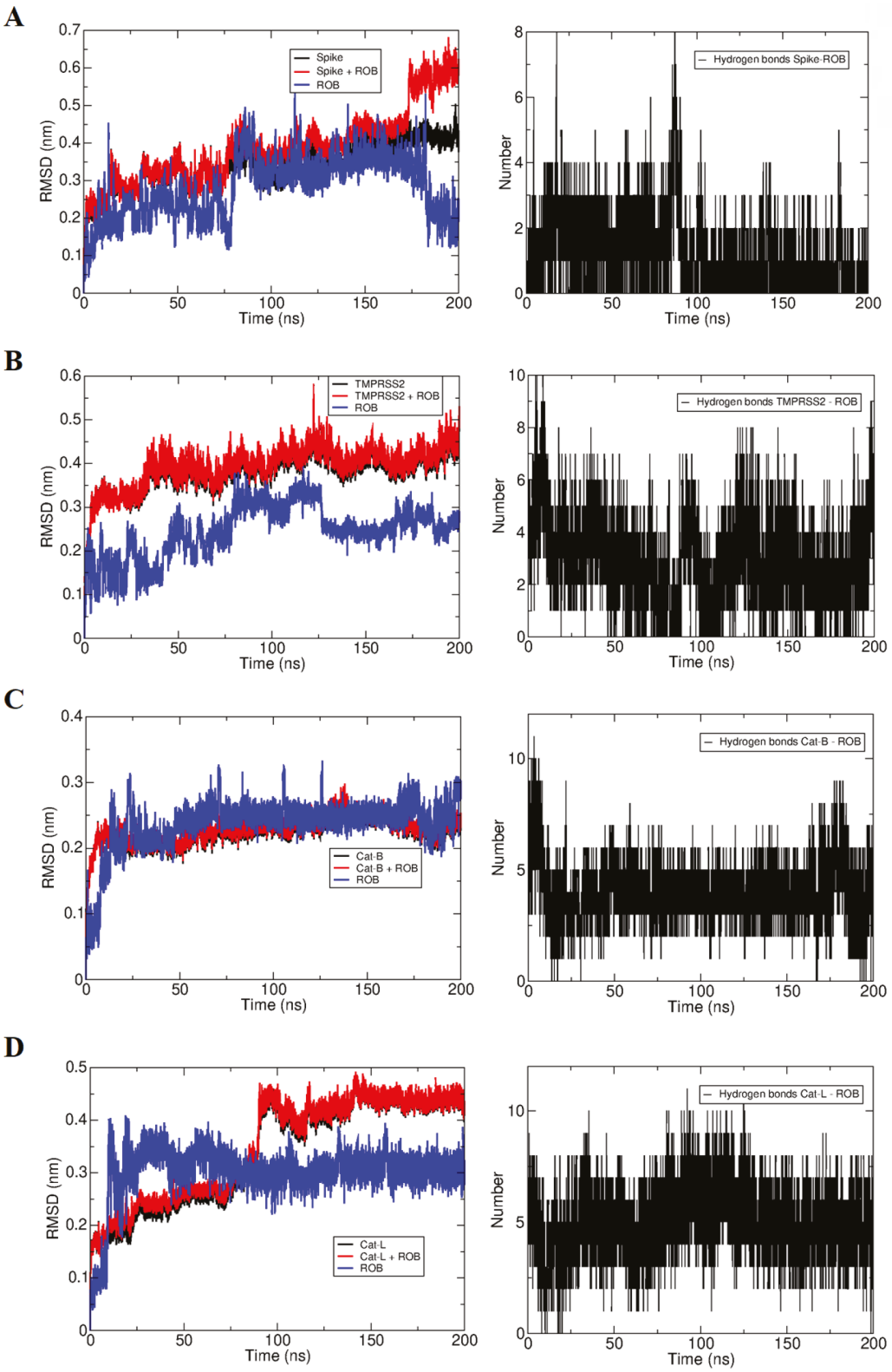

Figure 5. Time-dependent evolution of the structure and interactions of the robinin (ROB) molecule with target proteins in molecular dynamics analysis. A- RBD-ROB complex, B- TMPRSS2-ROB complex, C-CatB-ROB complex, D-CatL-ROB complex. On the left, the RMSD of the atomic positions of the receptor (black), ligand (blue), and the ligand + receptor (red) complex is given, while the right of the figure shows the number of hydrogen bonds between the ligand and the receptor.

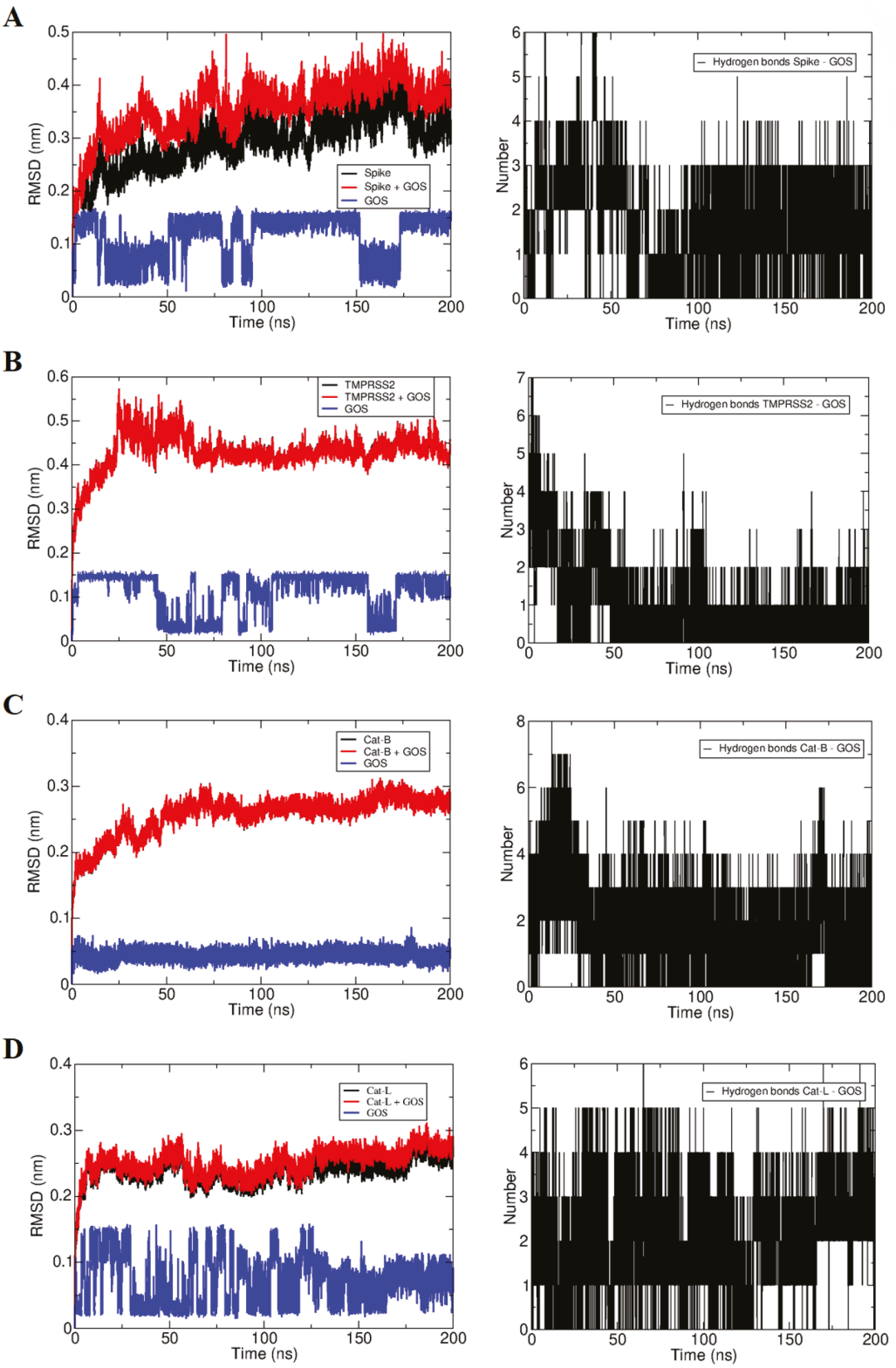

Figure 6. Time-dependent evolution of the structure and interactions of the gossypetin (GOS) molecule with target proteins in molecular dynamics analysis. A- RBD-GOS complex, B- TMPRSS2-GOS complex, C-CatB-GOS complex, D-CatL-GOS complex. On the left, the RMSD of the atomic positions of the receptor (black), ligand (blue), and the ligand + receptor (red) complex is given, while the right of the figure shows the number of hydrogen bonds between the ligand and the receptor.

energy of a system is calculated as a sum of contributions (bond, angle, dihedral, electrostatic, van der Waals, polar, and nonpolar solvation terms and entropy estimation) (Kollman et al., 2000). The binding free energy is calculated as a difference between the calculated free energies of complex (protein + ligand) and the free energies of the isolated protein and ligand, sampled over a large number of configurations, usually generated using molecular dynamics simulations. In the MM/PBSA method the Poisson–Boltzmann equation is used to calculate the polar solvation free energy contribution, whereas in the MM/GBSA method the (more simplified but faster) generalized Born model is employed for this purpose. Both methods yield similar results and their merits are discussed in the recent literature (Genheden and Ryde 2015; Sun et al., 2018). Being fully compatible with GROMACS as an additional program with GROMACS-like syntax, we employed the g_mmpbsa program which applies MM/PBSA method to molecular dynamics trajectories (Kumari et al., 2014).

In our study, the results obtained from docking and molecular dynamic analysis and the binding free energy values calculated by the MM/PBSA (Table 4) method corroborate each other. As evidenced by the negative binding free energies, ROB had favorable interactions with all other receptors. The ROB molecule made its strongest interaction with the CatB, while the weakest interaction was made with the TMPRSS2. These results are in agreement with the time-dependent evolution of the number of hydrogen bonds and qualitative analysis of simulations. Likewise, for GOS, MM/PBSA, docking, and molecular dynamics results support each other. The interactions of GOS with all receptors are favorable. While GOS performed its strongest interaction with CatB, the weakest interaction was found for GOS with spike glycoprotein. These results are consistent with the time-dependent evolution of the number of hydrogen bonds and qualitative analysis of the simulations. It is noteworthy that the interaction between ROB and CatB could be described as very strong by all methods: docking scores, MM/PBSA free energy calculations and also by the qualitative analysis of the molecular dynamics simulations.

4. Discussion

According to the literature records, there is no report on the interactions of GOS, natsudaidain, kaempferide, amurensin, azalein, icariin, spiraeoside, and xanthorhamnin with the target proteins in this study. On the other hand, there are studies that examine the inhibitory potentials of 3-hydroxyflavone (Batool et al., 2020), fisetin (Arora et al., 2020; Oladele et al., 2020), astragalin (Arora et al., 2020), morine (Laskar et al., 2020), galangin (Hashem, 2020), pachypodol (Ebada et al., 2020), rhamnazin (Swargiary et al., 2020), rhamnetin (Fischer

Table 4. Free energies of binding and their components, calculated using MM/PBSA, for the interaction between robinin, gossypetin and the receptors A- Spike, B- TMPRSS2, C- CatB and D- CatL.

Ligand	Protein	Van der Waals Energy (kj/mol)	Electrostatic energy (kj/mol)	Polar solvation energy (kj/mol)	SASA energy (kj/mol)	Binding energy (kj/mol)
Robinin	Spike	-133.914 +/- 1.770 kJ/mol	-29.898 +/- 1.482 kJ/mol	118.541 +/- 3.002 kJ/mol	-14.707 +/- 0.253 kJ/mol	-59.879 +/- 1.585 kJ/mol
	TMPRSS2	-203.769 +/- 2.168 kJ/mol	-74.785 +/- 1.941kJ/mol	243.174 +/- 3.185 kJ/mol	-22.268 +/- 0.138 kJ/mol	-57.828 +/- 2.318 kJ/mol
	CatB	-231.051 +/- 1.660 kJ/mol	-66.831 +/- 1.873 kJ/mol	177.507 +/- 2.599 kJ/mol	-23.652 +/- 0.125 kJ/mol	-144.115 +/- 1.317 kJ/mol
	CatL	-179.982 +/- 2.207 kJ/mol	-148.681 +/- 3.039 kJ/mol	252.426 +/- 4.883 kJ/mol	-22.524 +/- 0.215 kJ/mol	-98.687 +/- 1.634 kJ/mol
Gossypetin	Spike	-70.987 +/- 1.297 kJ/mol	-47.116 +/- 2.691 kJ/mol	80.120 +/- 2.538 kJ/mol	-8.853 +/- 0.083 kJ/mol	-46.843 +/- 1.127 kJ/mol
	TMPRSS2	-150.764 +/- 1.223 kJ/mol	-34.114 +/- 2.083 kJ/mol	117.266 +/- 1.747 kJ/mol	-13.473 +/- 0.097 kJ/mol	-81.049 +/- 1.154 kJ/mol
	CatB	-161.606 +/- 0.711 kJ/mol	-24.490 +/- 1.229 kJ/mol	89.835 +/- 1.166 kJ/mol	-14.946 +/- 0.058 kJ/mol	-111.257 +/- 0.732 kJ/mol
	CatL	-122.410 +/- 1.236 kJ/mol	-60.958 +/- 2.313 kJ/mol	101.533 +/- 2.105 kJ/mol	-12.594 +/- 0.061 kJ/mol	-94.330 +/- 1.046 kJ/mol

et al., 2020; Kousar et al., 2020), hyperoside (Cherrak et al., 2020; De Jesús-González et al., 2020; Hu et al., 2020), astragalin (Hu et al., 2020), myricitrin (Abd El-Mordy et al., 2020; Joshi et al., 2020), quercitrin (Arora et al., 2020; Patel et al., 2020), and troxerutin (Kandeel et al., 2020) on several proteins of SARS-CoV-2. However, there have been no studies observed investigating the inhibitory effect of the above-mentioned phytochemicals on spike glycoprotein, TMPRSS2, CatB, and CatL simultaneously.

According to the literature records, there is one report examining the interaction of only 3-hydroxyflavone, among flavonols examined in the present study, with TMPRSS2 (Puttaswamy et al., 2020). According to this study, quercetin 3,5-diglucoside (–9.6 kcal/mol), myricetin 3-rutinoside (–9.4 kcal/mol), rutin (–9.3 kcal/mol), kaempferol (–9.2 kcal/mol), myricetin 3-rhamnoside (–9.2 kcal/mol), and robinetin 3-rutinoside (–9.6 kcal/mol) originating from the 3-hydroxyfavone chemical structure exhibited highly favorable binding free energies against TMPRSS2. These values were higher than the value (–5.68 kcal/mol) presented in the current study. It was thought that this difference may be due to minor differences in the glycosidic structures of the flavonols in question.

The flavonols examined in the present study were also subjected to literature research in terms of their interactions with spike glycoprotein of SARS-CoV-2. It was determined that the interactions of flavonols except fiset in (Jain et al., 2021; Vijayakumar et al., 2020), galang in (Jain et al., 2021), morin (Jain et al., 2021), astragalin (Adejoro et al., 2020; Hiremath et al., 2021), kaempferitrin (Arokiyaraj et al., 2020), quercitrin (Teli et al., 2020; Hiremath et al., 2021), and troxerutin (Somadi and Sivan, 2020) with spike glycoprotein were not analyzed. It is of course impossible to discuss here all of the data presented in these reports. In general, however, the binding free energy data obtained for flavonols given above appear to be consistent with those presented in the current study. It was thought that the negligible differences between the literature data and the existing data may be due to the use of different docking programs for in silico analysis.

On the other hand, the ROB molecule extracted from *Platycodi radix*, the root of the *Platycodon grandiflorum* plant, has been reported to bind to the 3CL pro enzyme of SARS-CoV-2 and to inhibit its proteolytic activity (Leung et al., 2020). In addition, in a different study carried out using the molecular docking method, gossypetin-3'-O-glucoside, a GOS derivative, has been reported to show highly favorable inhibitory potential (ΔG: –11.93 kcal/mol) by binding to Cys145 and His41 residues in the catalytic center of 3CLpro (Giguet-Valard et al., 2020). We are in the opinion that the reason behind the high affinity of ROB and GOS for the spike, TMPRSS2, CatB, and CatL enzymes in our computational study is that: hydrogen (H) bonds formed between the H atoms attached to -OH groups of ROB and GOS and the electron pairs on heteroatoms (such as N, O) of 4 different enzymes increase the stability of the receptor-ligand interactions. In a similar mechanism, the H-bonds formed between the electron pairs on the C=O (carbonyl) or oxygen atom (–O–) of ROB and GOS and the H atoms bound to the heteroatoms (such as N, O) of these 4 different enzymes also favor the stability of the receptor-ligand interactions.

As can be seen from the sections above, ROB and GOS were announced as 'hit' flavonols. No other computational study has been found investigating the inhibition potential of the ROB on a different virus other than SARS-CoV-2. However, there are some reports that GOS has antiviral activity on chikungunya virus (CHIKV), dengue virus (DENV), and Ebola virus (EBOV)(Raj and Varadwaj, 2016; Keramagi and Skariyachan, 2018). In a study by Keramagi and Skariyachan (2018), it was reported that GOS exhibited the most negative binding energy (kcal/mol) and maximum stabilizing interactions on CHIKV and DENV targets. In another study by Raj and Varadwaj (2016), it was reported that GOS exhibited highly significant docking scores on EBOV receptor proteins. These literature findings indicate that GOS has a high antiviral activity potential.

5. Conclusion

According to the results obtained from this study, ROB and GOS showed promising activities on the RBD of the spike glycoprotein of 2019-nCoV, TMPRSS2, and cathepsins. The employed methods (molecular docking, MM/PBSA free energy estimates, and qualitative MD analysis) are in close agreement in almost all cases. In particular, a remarkable strong interaction was found between ROB and CatB. Therefore, it has been concluded that these molecules can be considered as an alternative approach in the treatment of COVID-19 disease. Although these molecules showed neither AMES toxicity nor hepatotoxicity, it was thought-provoking that GOS has an inhibitory effect on CYPs and that ROB is a substrate of P-gp. However, according to SwissADME database, GOS still meets the criteria for drug likeness and, more importantly, lead likeness. Moreover, our other hit ligand, ROB, has been proven to be used as a reliable antidiabetic agent in an in vivo study, and as an antiinflammatory and antiarthritic drug in a different in vivo study (Srivastava et al., 2017; Tsiklauri et al., 2021). It was concluded that further in vitro and/or in vivo tests should be performed in order to reveal the ultimate toxicity of the molecules in question and their effects on cellular energy metabolism, and if necessary, the observed side effects should be minimized by molecular modifications.

Thus, the theoretical data could hopefully be confirmed experimentally.

Acknowledgments
P.A.N. would like to thank CNPq (Bolsa de Produtividade) and CAPES (Financial code 001) for financial support and Centro Nacional de Supercomputação (CESUP), Universidade Federal do Rio Grande do Sul (UFRGS) for providing HPC resources.

Conflict of interest
The authors declare no competing financial interest.

References

Abd El-Mordy FM, El-Hamouly MM, Ibrahim MT, Abd El-Rheem G, Aly OM et al. (2020). Inhibition of SARS-CoV-2 main protease by phenolic compounds from Manilkara hexandra (Roxb.) Dubard assisted by metabolite profiling and in silico virtual screening. RSC Advances 10: 32148-32155.

Abraham MJ, Murtola T, Schulz R, Páll S, Smith JC et al. (2015). GROMACS: high performance molecular simulations through multi-level parallelism from laptops to supercomputers. SoftwareX 1-2: 19-25.

Adejoro IA, Babatunde DD, Tolufashe GF (2020). Molecular docking and dynamic simulations of some medicinal plants compounds against SARS-CoV-2: an in silico study. Journal of Taibah University for Science 14: 1563-1570.

Andersen KG, Rambaut A, Lipkin WI, Holmes EC, Garry RF (2020). The proximal origin of SARS-CoV-2. Nature Medicine 26: 450-452.

Arokiyaraj S, Stalin A, Kannan BS, Shin H (2020). Geranii Herba as a potential inhibitor of SARS-CoV-2 main 3CLpro, spike RBD, and regulation of unfolded protein response: an in silico approach. Antibiotics 9: 863.

Arora S, Lohiya G, Moharir K, Shah S, Yende S (2020). Identification of potential flavonoid inhibitors of the SARS-CoV-2 main protease 6YNQ: a molecular docking study. Digital Chinese Medicine 3: 239-248.

Baker NA, Sept D, Joseph S, Holst MJ, McCammon JA (2001). Electrostatics of nanosystems: application to microtubules and the ribosome. Proceedings of the National Academy of Sciences 98: 10037-10041.

Batool F, Mughal EU, Zia K, Sadiq A, Naeem N et al. (2020). Synthetic flavonoids as potential antiviral agents against SARS-CoV-2 main protease. Journal of Biomolecular Structure and Dynamics (In press). doi: 10.1080/07391102.2020.1850359

Camacho C, Coulouris G, Avagyan V, Ma N, Papadopoulos J et al. (2009). BLAST+: architecture and applications. BMC Bioinformatics 10: 421.

Cannalire R, Stefanelli I, Cerchia C, Beccari AR, Pelliccia S et al. (2020). SARS-CoV-2 entry inhibitors: small molecules and peptides targeting virus or host cells. International Journal of Molecular Sciences 21: 5707.

Cataneo AHD, Kuczera D, Koishi AC, Zanluca C, Silveira GF et al. (2019). The citrus flavonoid naringenin impairs the in vitro infection of human cells by Zika virus. Scientific Reports 9: 16348.

Chan-Yeung M, Xu RH (2003). SARS: epidemiology. Respirology 8: S9-S14.

Chan JF-W, Kok K-H, Zhu Z, Chu H, To KK-Wet al. (2020). Genomic characterization of the 2019 novel human-pathogenic coronavirus isolated from a patient with atypical pneumonia after visiting Wuhan. Emerging Microbes & Infections 9: 221-236.

Chen M, Chen XX, Song X, Muhammad A, Jia RY et al. (2019). The immune-adjuvant activity and the mechanism of resveratrol on pseudorabies virus vaccine in a mouse model. International Immunopharmacology 76: 105876.

Chen Y, Li P, Su SJ, Chen M, He J et al. (2019). Synthesis and antibacterial and antiviral activities of myricetin derivatives containing a 1,2,4-triazole Schiff base. RSC Advances 9: 23045-23052.

Cherrak SA, Merzouk H, Mokhtari-Soulimane N (2020). Potential bioactive glycosylated flavonoids as SARS-CoV-2 main protease inhibitors: a molecular docking and simulation studies. Plos One 15: e0240653.

Colovos C, Yeates TO (1993). Verification of protein structures: patterns of nonbonded atomic interactions. Protein Science 2: 1511-1519.

Dai WW, Bi JP, Li F, Wang S, Huang XY et al. (2019). Antiviral efficacy of flavonoids against enterovirus 71 infection in vitro and in newborn mice. Viruses 11: 625.

Daina A, Michielin O, Zoete V (2017). SwissADME: a free web tool to evaluate pharmacokinetics, drug-likeness and medicinal chemistry friendliness of small molecules. Scientific Reports 7: 42717.

Daina A, Michielin O, Zoete V (2019). SwissTarget prediction: updated data and new features for efficient prediction of protein targets of small molecules. Nucleic Acids Research 47: W357-W364.

Darden T, York D, Pedersen L (1993). Particle mesh Ewald: an N·log(N) method for Ewald sums in large systems. The Journal of Chemical Physics 98: 10089-10092.

Dávalos A, Castilla P, Gómez-Cordovés C, Bartolomé B (2006). Quercetin is bioavailable from a single ingestion of grape juice. International Journal of Food Sciences and Nutrition 57: 391-398.

De Andrade J, Gonçalves PFB, Netz PA (2021). Why does the novel coronavirus spike protein interact so strongly with the human ACE2? A thermodynamic answer. ChemBioChem 22: 865-875. doi.org/10.1002/cbic.202000455

Jesús-González LAD, Osuna-Ramos JF, Reyes-Ruiz JM, et al. (2020). Flavonoids and nucleotide analogs show high affinity for viral proteins of SARS-CoV-2 by in silico analysis: new candidates for the treatment of COVID-19. Research Square (Preprint). doi: 10.21203/rs.3.rs-67272/v1.

Del Barrio G, Spengler I, Garcia T, Roque A, Alvarez AL et al. (2011). Antiviral activity of *Ageratina havanensis* and major chemical compounds from the most active fraction. Revista Brasileira De Farmacognosia 21: 915-920.

Delaney JS (2004). ESOL: estimating aqueous solubility directly from molecular structure. Journal of Chemical Information and Computer Sciences 44: 1000-1005.

Duan CJ, Xian L, Zhao GC, Feng Y, Pang Het al. (2009). Isolation and partial characterization of novel genes encoding acidic cellulases from metagenomes of buffalo rumens. Journal of Applied Microbiology 107: 245-256.

Dwivedi VD, Bharadwaj S, Afroz S, Khan N, Ansari MA et al. (2020). Anti-dengue infectivity evaluation of bioflavonoid from *Azadirachta indica* by dengue virus serine protease inhibition. Journal of Biomolecular Structure & Dynamics. doi: 10.1080/07391102.07392020.01734485

Ebada SS, Al-Jawabri NA, Youssef FS, El-Kashef DH, Knedel T-O et al. (2020). Anti-inflammatory, antiallergic and COVID-19 protease inhibitory activities of phytochemicals from the Jordanian hawksbeard: identification, structure–activity relationships, molecular modeling and impact on its folk medicinal uses. RSC Advances 10: 38128-38141.

Essmann U, Perera L, Berkowitz ML, Darden T, Lee H et al. (1995). A smooth particle mesh Ewald method. The Journal of Chemical Physics 103: 8577-8593.

Fischer A, Sellner M, Neranjan S, Smieško M, Lill MA (2020). Potential inhibitors for novel coronavirus protease identified by virtual screening of 606 million compounds. International Journal of Molecular Sciences 21: 3626.

Genheden S, Ryde U (2015). The MM/PBSA and MM/GBSA methods to estimate ligand-binding affinities. Expert Opinion on Drug Discovery 10: 449-461.

Giguet-Valard A-G, Raguette K, Morin S, Bellance R, Ravin JS (2020). Gossypetin derivatives are also putative inhibitors of SARS-CoV-2: results of a computational study. Journal of Biomedical Research & Environmental Sciences 1: 201-212.

Greenspan PD, Clark KL, Tommasi RA, Cowen SD, McQuire LW et al. (2001). Identification of dipeptidyl nitriles as potent and selective inhibitors of cathepsin B through structure-based drug design. Journal of Medicinal Chemistry 44: 4524-4534.

Guex N, Peitsch MC, Schwede T (2009). Automated comparative protein structure modeling with SWISS-MODEL and Swiss-PdbViewer: a historical perspective. Electrophoresis 30: S162-S173.

Hardegger LA, Kuhn B, Spinnler B, Anselm L, Ecabert R et al.(2011). Halogen bonding at the active sites of human cathepsin L and MEK1 kinase: efficient interactions in different environments. ChemMedChem 6: 2048-2054.

Hashem HE (2020). In silico approach of some selected honey constituents as SARS-CoV-2 main protease (COVID-19) inhibitors. Eurasian Journal of Medicine and Oncology 4: 196-200.

Hiremath S, Kumar HV, Nandan M, Mantesh M et al. (2021). In silico docking analysis revealed the potential of phytochemicals present in Phyllanthus amarus and Andrographis paniculata, used in Ayurveda medicine in inhibiting SARS-CoV-2. 3 Biotechnology 11: 1-18.

Homeyer N, Gohlke H (2012). Free energy calculations by the molecular mechanics Poisson-Boltzmann surface area method. Molecular Informatics 31: 114-122.

Hoover WG (1985). Canonical dynamics: equilibrium phase-space distributions. Physical Review A 31: 1695-1697.

Hu X, Cai X, Song X, Li C, Zhao Jet al. (2020). Possible SARS-coronavirus 2 inhibitor revealed by simulated molecular docking to viral main protease and host toll-like receptor. Future Virology 15: 359-368.

Huang C, Wang Y, Li X, Ren L, Zhao Jet al. (2020). Clinical features of patients infected with 2019 novel coronavirus in Wuhan, China. The Lancet 395: 497-506.

Istifli ES, Netz PA, Sihoglu Tepe A, Husunet MT, Sarikurkcu C et al. (2020). In silico analysis of the interactions of certain flavonoids with the receptor-binding domain of 2019 novel coronavirus and cellular proteases and their pharmacokinetic properties. Journal of Biomolecular Structure and Dynamics 1-15. (In press). doi: 10.1080/07391102.2020.1840444

Istifli ES, Sihoglu Tepe A, Sarikurkcu C, Tepe B (2020). Interaction of certain monoterpenoid hydrocarbons with the receptor-binding domain of 2019 novel coronavirus (2019-nCoV), transmembrane serin protease 2 (TMPRSS2), cathepsin B, and cathepsin L (CatB/L) and their pharmacokinetic properties. Turkish Journal of Biology 44: 242-264.

Iwata-Yoshikawa N, Okamura T, Shimizu Y, Hasegawa H, Takeda M et al. (2019). TMPRSS2 contributes to virus spread and immunopathology in the airways of murine models after coronavirus infection. Journal of Virology 93.

Jain AS, Sushma P, Dharmashekar C, Beelagi MS, Prasad SK et al. (2021). In silico evaluation of flavonoids as effective antiviral agents on the spike glycoprotein of SARS-CoV-2. Saudi Journal of Biological Sciences 28: 1040-1051.

Jakalian A, Jack DB, Bayly CI (2002). Fast, efficient generation of high-quality atomic charges. AM1-BCC model: II. Parameterization and validation. Journal of Computational Chemistry 23: 1623-1641.

Jorgensen WL, Chandrasekhar J, Madura JD, Impey RW, Klein ML (1983). Comparison of simple potential functions for simulating liquid water. The Journal of Chemical Physics 79: 926-935.

Joshi R, Jagdale S, Bansode S, Shankar SS, Tellis M et al. (2020). Discovery of potential multi-target-directed ligands by targeting host-specific SARS-CoV-2 structurally conserved main protease. Journal of Biomolecular Structure and Dynamics. doi: 10.1080/07391102.2020.1760137

Kandeel M, Kitade Y, Almubarak A (2020). Repurposing FDA-approved phytomedicines, natural products, antivirals and cell protectives against SARS-CoV-2 (COVID-19) RNA-dependent RNA polymerase. PeerJ 8: e10480.

Kawase M, Shirato K, Van der Hoek L, Taguchi F, Matsuyama S (2012). Simultaneous treatment of human bronchial epithelial cells with serine and cysteine protease inhibitors prevents severe acute respiratory syndrome coronavirus entry. Journal of Virology 86: 6537-6545.

Keramagi AR, Skariyachan S (2018). Prediction of binding potential of natural leads against the prioritized drug targets of chikungunya and dengue viruses by computational screening. 3 Biotech 8 (6): 14.

Kollman PA, Massova I, Reyes C, Kuhn B, Huo S et al. (2000). Calculating structures and free energies of complex molecules: combining molecular mechanics and continuum models. Accounts of Chemical Research 33: 889-897.

Kousar K, Majeed A, Yasmin F, Hussain W, Rasool N (2020). Phytochemicals from selective plants have promising potential against SARS-CoV-2: investigation and corroboration through molecular docking, MD simulations, and quantum computations. BioMed Research International 2020: 6237160.

Kumari R, Kumar R, Lynn A (2014). g_mmpbsa—a GROMACS tool for high-throughput MM-PBSA calculations. Journal of Chemical Information and Modeling 54: 1951-1962.

Kumari R, Kumar R. Open Source Drug Discovery C, Lynn A (2014). g_mmpbsa--a GROMACS tool for high-throughput MM-PBSA calculations. Journal of Chemical Information and Modeling 54: 1951-1962.

Lan J, Ge J, Yu J, Shan S, Zhou Het al. (2020). Structure of the SARS-CoV-2 spike receptor-binding domain bound to the ACE2 receptor. Nature 581: 215-220.

Laskar MA, Begam M, Dutta Choudhury M. In silico screening of some antiviral phytochemicals as drug leads against Covid-19. ChemRxiv Preprint 2020. doi: 10.26434/chemrxiv.12478568.v

Laskowski RA, MacArthur MW, Moss DS, Thornton JM (1993). PROCHECK: a program to check the stereochemical quality of protein structures. Journal of Applied Crystallography 26: 283-291.

LeCher JC, Diep N, Krug PW, Hilliard JK (2019). Genistein has antiviral activity against herpes B virus and acts synergistically with antiviral treatments to reduce effective dose. Viruses 11: E499.

Leung EL, Pan HD, Huang YF, Fan XX, Wang WY et al. (2020). The Scientific Foundation of Chinese Herbal Medicine against COVID-19. Engineering (Beijing) 6: 1099-1107.

Ling LJ, Lu Y, Zhang YY, Zhu HY, Tu P et al. (2020). Flavonoids from *Houttuynia cordata* attenuate H1N1-induced acute lung injury in mice via inhibition of influenza virus and toll-like receptor signaling. Phytomedicine 67: 153150.

Lopes BRP, Da Costa MF, Ribeiro AG, Da Silva TF, Lima CS et al. (2020). Quercetin pentaacetate inhibits in vitro human respiratory syncytial virus adhesion. Virus Research 276: 197805.

Memish ZA, Perlman S, Van Kerkhove MD, Zumla A (2020). Middle East respiratory syndrome. The Lancet 395: 1063-1077.

Mohd A, Zainal N, Tan KK, AbuBakar S (2019). Resveratrol affects Zika virus replication *in vitro*. Scientific Reports 9: 14336.

Morris GM, Huey R, Lindstrom W, Sanner MF, Belew RK et al. (2009). AutoDock4 and AutoDockTools4: automated docking with selective receptor flexibility. Journal of Computational Chemistry 30: 2785-2791.

Morris GM, Lim-Wilby M (2008). Molecular docking. In: Kukol A (Ed.) Molecular Modeling of Proteins. Springer, Switzerland, pp. 365-382.

Nagai E, Iwai M, Koketsu R, Okuno Y, Suzuki Y et al. (2019). Anti-influenza virus activity of adlay tea components. Plant Foods for Human Nutrition 74: 538-543.

Nasab RR, Hassanzadeh F, Khodarahmi GA, Rostami M, Mirzaei M et al. (2017). Docking study, synthesis and antimicrobial evaluation of some novel 4-anilinoquinazoline derivatives. Research in Pharmaceutical Sciences 12: 425-433.

O'Boyle NM, Banck M, James CA, Morley C, Vandermeersch T et al. (2011). Open Babel: an open chemical toolbox. Journal of Cheminformatics 3: 33.

Oladele JO, Oyeleke OM, Oladele OT, Olowookere BD, Oso BJ et al. (2020). Kolaviron (Kolaflavanone), apigenin, fisetin as potential Coronavirus inhibitors: in silico investigation. Research Square. doi: 10.21203/rs.3.rs-51350/v1

Omotuyi IO, Nash O, Ajiboye OB, Iwegbulam CG, Oyinloye EB et al. (2020). Atomistic simulation reveals structural mechanisms underlying D614G spike glycoprotein-enhanced fitness inSARS-COV-2. Journal of Computational Chemistry 41: 2158-2161.

Parrinello M, Rahman A (1981). Polymorphic transitions in single crystals: a new molecular dynamics method. Journal of Applied Physics 52: 7182-7190.

Parvez MK, Rehman MT, Alam P, Al-Dosari MS, Alqasoumi SI et al. (2019). Plant-derived antiviral drugs as novel hepatitis B virus inhibitors: cell culture and molecular docking study. Saudi Pharmacological Journal 27: 389-400.

Patel R, Vanzara A, Patel N, Vasava A, Patil S et al. (2020). Discovery of fungal metabolites bergenin, quercitrin and dihydroartemisinin as potential inhibitors against main protease of SARS-CoV-2. Biological and Medicinal Chemistry (preprint).

Pedretti A, Villa L, Vistoli G (2004). VEGA–an open platform to develop chemo-bio-informatics applications, using plug-in architecture and script programming. Journal of Computer-Aided Molecular Design 18: 167-173.

Perez-Vizcaino F, Duarte J (2010). Flavonols and cardiovascular disease. Molecular Aspects of Medicine 31: 478-494.

Pires DE, Blundell TL, Ascher DB (2015). pkCSM: predicting small-molecule pharmacokinetic and toxicity properties using graph-based signatures. Journal of Medicinal Chemistry 58: 4066-4072.

Puttaswamy H, Gowtham HG, Ojha MD, Yadav A, Choudhir G et al. (2020). In silico studies evidenced the role of structurally diverse plant secondary metabolites in reducing SARS-CoV-2 pathogenesis. Scientific Reports 10: 1-24.

Raj U, Varadwaj PK (2016). Flavonoids as multi-target inhibitors for proteins associated with ebola virus: in silico discovery using virtual screening and molecular docking studies. Interdisciplinary Sciences-Computational Life Sciences 8: 132-141.

Remmert M, Biegert A, Hauser A, Söding J (2012). HHblits: lightning-fast iterative protein sequence searching by HMM-HMM alignment. Nature Methods 9: 173-175.

Richman DD, Whitley RJ, Hayden FG (2016). Clinical virology, 4th ed. John Wiley & Sons.

Ritta M, Marengo A, Civra A, Lembo D, Cagliero C et al. (2020). Antiviral activity of a *Arisaema tortuosum* leaf extract and some of its constituents against herpes simplex virus type 2. Planta Medica 86: 267-275.

Sanner MF (1999). Python: a programming language for software integration and development. Journal of Molecular Graphics and Modelling 17: 57-61.

Sharma S (1996). Two group discriminant analysis. Applied Multivariate Techniques: 237-286.

Shirato K, Kanou K, Kawase M, Matsuyama S (2017). Clinical isolates of human coronavirus 229E bypass the endosome for cell entry. Journal of Virology 91.

Shirato K, Kawase M, Matsuyama S (2018). Wild-type human coronaviruses prefer cell-surface TMPRSS2 to endosomal cathepsins for cell entry. Virology 517: 9-15.

Simmons G, Gosalia DN, Rennekamp AJ, Reeves JD, Diamond SL et al. (2005). Inhibitors of cathepsin L prevent severe acute respiratory syndrome coronavirus entry. Proceedings of the National Academy of Sciences 102: 11876-11881.

Singhal T (2020). A review of coronavirus disease-2019 (COVID-19). Indian Journal of Pediatrics 87: 281-286.

Sochocka M, Sobczynski M, Ochnik M, Zwolinska K, Leszek J (2019). Hampering herpesviruses HHV-1 and HHV-2 infection by extract of *Ginkgo biloba* (EGb) and its phytochemical constituents. Frontiers in Microbiology 10: 2367.

Somadi G, Sivan SK (2020). Identification of therapeutic target in S2 domain of SARS nCov-2 spike glycoprotein: key to design and discover drug candidates for inhibition of viral entry into host cell. Journal of Theoretical and Computational Chemistry 19: 2050028.

Sousa da Silva AW, Vranken WF (2012). ACPYPE - AnteChamber PYthon Parser interfacE. BMC Research Notes 5: 367.

Srivastava S, Shree P, Tripathi YB (2017). Active phytochemicals of Pueraria tuberosa for DPP-IV inhibition: in silico and experimental approach. Journal of Diabetes & Metabolic Disorders 16: 46.

Studer G, Rempfer C, Waterhouse AM, Gumienny R, Haas J et al. (2020). QMEANDisCo—distance constraints applied on model quality estimation. Bioinformatics 36: 1765-1771.

Sun H, Duan L, Chen F, Liu H, Wang Z et al. (2018). Assessing the performance of MM/PBSA and MM/GBSA methods. 7. Entropy effects on the performance of end-point binding free energy calculation approaches. Physical Chemistry Chemical Physics 20: 14450-14460.

Swargiary A, Mahmud S, Saleh MA (2020). Screening of phytochemicals as potent inhibitor of 3-chymotrypsin and papain-like proteases of SARS-CoV2: an in silico approach to combat COVID-19. Journal of Biomolecular Structure and Dynamics. doi: 10.1080/07391102.2020.1835729

Tang X, Zhang C, Chen M, Xue YN, Liu TT et al. (2020). Synthesis and antiviral activity of novel myricetin derivatives containing ferulic acid amide scaffolds. New Journal of Chemistry 44: 2374-2379.

Teli DM, Shah MB, Chhabria MT (2020). In silico screening of natural compounds as potential inhibitors of SARS-CoV-2 main protease and spike receptor-binding domain bound with ACE2 COVID-19 target proteins. Frontiers in Molecular Biosciences 7: 429.

Trujillo-Correa AI, Quintero-Gil DC, Diaz-Castillo F, Quinones W, Robledo SM et al. (2019). *In vitro* and *in silico* anti-dengue activity of compounds obtained from *Psidium guajava* through bioprospecting. BMC Complementary and Alternative Medicine 19: 298.

Tsiklauri L, Svik K, Chrastina M, Ponist S, Drafi F et al. (2021). Bioflavonoid robinin from *Astragalus falcatus* Lam. mildly improves the effect of metothrexate in rats with adjuvant arthritis. Nutrients 13: 1268.

Vazquez-Calvo A, De Oya NJ, Martin-Acebes MA, Garcia-Moruno E, Saiz JC (2017). Antiviral properties of the natural polyphenols delphinidin and epigallocatechin gallate against the flaviviruses West Nile virus, Zika virus, and Dengue virus. Frontiers in Microbiology 8: 1314.

Vijayakumar BG, Ramesh D, Joji A, Kannan T (2020). In silico pharmacokinetic and molecular docking studies of natural flavonoids and synthetic indole chalcones against essential proteins of SARS-CoV-2. European Journal of Pharmacology 886: 173448.

Vistoli G, Pedretti A, Testa B (2008). Assessing drug-likeness--what are we missing? Drug Discovery Today 13: 285-294.

Wang J, Wolf RM, Caldwell JW, Kollman PA, Case DA (2004). Development and testing of a general amber force field. Journal of Computational Chemistry 25: 1157-1174.

Wang R, Zhang X, Irwin DM, Shen Y (2020). Emergence of SARS-like coronavirus poses new challenge in China. Journal of Infection 80: 350-371.

Wang Y, Liu M, Gao J (2020). Enhanced receptor binding of SARS-CoV-2 through networks of hydrogen-bonding and hydrophobic interactions. Proceedings of the National Academy of Sciences 117: 13967-13974.

Wilson S, Greer B, Hooper J, Zijlstra A, Walker B et al. (2005). The membrane-anchored serine protease, TMPRSS2, activates PAR-2 in prostate cancer cells. Biochemical Journal 388: 967-972.

Woo H, Park SJ, Choi YK, Park T, Tanveer M et al. (2020). Developing a fully glycosylated full-length SARS-CoV-2 spike protein model in a viral membrane. The Journal of Physical Chemistry B.

Zakaryan H, Arabyan E, Oo A, Zandi K (2017). Flavonoids: promising natural compounds against viral infections. Archives of Virology 162: 2539-2551.

Zhou Y, Vedantham P, Lu K, Agudelo J, Carrion Jr R et al. (2015). Protease inhibitors targeting coronavirus and filovirus entry. Antiviral Research 116: 76-84.

Supplementary

Contents

Method

Structural optimization of ligands

The protein data bank (pdb) files of all twenty-three ligands (3-hydroxyflavone, azaleatin, galangin, gossypetin, kaempferide, natsudaidain, pachypodol, rhamnazin, amurensin, fisetin, astragalin, azalein, morin, hyperoside, icariin, rhamnetin, myricitrin, kaempferitrin, quercitrin, robinin, troxerutin, spiraeoside, and xanthorhamnin) have been downloaded from PubChem (https://pubchem.ncbi.nlm.nih.gov/). The atom types and partial charges of the ligands were optimized with MMFF94 force field using the Avogadro software.

Energy minimization of 2019-nCoV ACE2-RBD, TMPRSS2, CatB/L using nanoscale molecular dynamics (NAMD)

The structure of the spike glycoprotein was gained by removing the ACE2 subunit from the angiotensin-converting enzyme 2-2019nCoV RBD complex in the Vega ZZ software (Pedretti et al., 2004). This model was downloaded from the following URL: https://swissmodel.expasy.org/interactive/HLkhkP/models/03 (PDBID: model_03.pdb) (Camacho et al., 2009; Remmert et al., 2012). Since the structure of the spike glycoprotein in model_03 displayed a sequence identity of 100% to the 2019-nCoV ACE2 binding domain, this model was chosen as the appropriate 3D structure through molecular docking analyses. During the protein preparation step, the atom types and electrical charges of the spike glycoprotein were fixed using CHARMM22_PROT force field and Gasteiger–Marsili charges. Next, for the energy minimization of the spike glycoprotein with NAMD, each parameter was loaded from a template file. The number of time steps (number of minimization steps) were set to 10,000 and CHARMM22_PROT was set as the force field. When the energy minimization was completed, the 3D structure corresponding to the last minimization step was saved as the lowest energy conformation. Also, to keep the spike glycoprotein structurally closer to the original crystallographic data, atom constraints were also applied to the protein backbone. In the energy minimization of TMPRSS2, CatB, and CatL, the same steps described above for the minimization of the 2019-nCoV spike glycoprotein were applied.

Homology modeling of TMPRSS2

The crystallographic structure of human TMPRSS2 enzyme has not been resolved until today, therefore, a homology model generated for this enzyme to utilize in further molecular docking and molecular dynamics analyses. The amino acid sequence of TMPRSS2 was downloaded from UniProtKB (https://www.uniprot.org/uniprot/O15393). Template search for TMPRSS2 catalytic domain was performed against the SWISS-MODEL template library with BLAST and HHBlits. BLAST was used to search the TMPRSS2 catalytic domain target sequence against the primary amino acid sequence in the SMTL (Remmert et al., 2012).

ProMod3 was used to carry out model building for TMPRSS2 catalytic domain based on the target-template alignment. The rest of the procedure was carried out as previously described (Guex et al., 2009).

The model quality (global and per-residue) of TMPRSS2 obtained was evaluated with the QMEAN scoring function (Studer et al., 2020). A near-zero QMEAN score was a good value in terms of the quality of the fit between model structure and the experimental structure. According to the QMEAN score, however, scores of 4.0 and below indicated that the model was of poor quality. Therefore, among the top 5 TMPRSS2 models we obtained as a result of homology modeling, we determined the 5ce1.1.A (model 06) model as the target structure in the molecular docking analysis.

In addition, whether our model has an energetically favorable conformation, we generated a Ramachandran plot (Figure S1) using the PROCHECK web server (Laskowski et al., 1993). Also, ERRAT web-based tool (Figure S2) was also deployed to calculate the overall quality factor (OQF) for nonbonded atomic interactions (Colovos and Yeates, 1993).

Molecular docking studies

Firstly, we think that it may be of importance to clarify the expressions of RBM (receptor binding motif) and RBD (receptor binding domain) of the spike protein: spike's RBD is the smallest part of this protein that is able to interact with the receptor, hACE2. The RBD consists of a core (residues 333-438 and residues 507-527) and the receptor binding motif (RBM, residues 438-506). This RBM is the part of the RBD that directly interacts with hACE2 (De Andrade et al., 2021; Lan et al., 2020; Omotuyi et al., 2020; Wang et al., 2020b; Woo et al., 2020). Therefore, we determined that RBM is a kind of "active site" of the RBD.

Molecular docking analyses between the target structures and the ligands were performed using AutoDock 4.2.6 and the corresponding docking scores (free energy of binding) of the ligands with 2019-nCoV RBM, TMPRSS2, CatB (PDB ID: 1GMY), and CatL (PDB ID: 2YJ9) were calculated. AutoDockTools-1.5.6 was used to prepare the target and ligand molecules and also the parameters prior to initiating the docking analysis using AutoDock 4.2.6 (Sanner, 1999b). In molecular docking studies, the grid box coordinates were adjusted to ensure that all the tested phytochemicals interact with amino acids in the active sites of the enzymes in question (Andersen et al., 2020a; Greenspan et al., 2001; Hardegger et al., 2011; Wilson et al., 2005).

Prior to molecular docking analyzes, polar hydrogen atoms in the receptor and the ligand molecules were retained, while nonpolar hydrogens were merged and then, the Gasteiger charges of the ligands were calculated with AutoDockTools (Morris et al., 2009; Nasab et al., 2017; Sanner, 1999a). Also, the Kollmann charges were added for the receptor. During the docking experiments, all the rotatable bonds of the ligands were allowed to rotate and then the optimized protein (rigid) and ligand (flexible) structures were saved in PDBQT format. Grid box coordinates were adjusted as: a) $80 \times 90 \times 40$ Å points for the spike glycoprotein; b) $60 \times 110 \times 86$ Å points for TMPRSS2; c) $86 \times 84 \times 44$ Å points for CatB; and d) $54 \times 52 \times 60$ Å points for CatL. These grid box sizes were previously determined to cover the active amino acid residues of the enzymes in question.

In all docking analyses, 100 genetic algorithm (GA) runs with an initial population of 150 individuals, maximum number of 2,500,000 energy evaluations, and a maximum number of 27,000 generations were selected. The values of 0.02 and 0.8 were chosen as the default parameters for mutation and crossover rates, respectively. After 100 independent docking runs, all the possible binding modes

(conformations) of the ligands were clustered by the program and were ranked based on the most negative binding free energy (kcal/mol) of the ligand conformation. The best docking poses obtained using the AutoDock 4.2.6 between the ligand and receptor structures were analyzed with the BIOVIA Discovery Studio v16.

Furthermore, according to the results obtained from molecular docking experiments, heatmaps of ligands (Supplementary Figures S3, S4, S5, and S6) that interact with specific amino acid residues of each receptor were created. Heatmaps are built on the logic of how many times each ligand interacts with each residue (regardless of bond type). Thus, heatmaps provide an overview of the frequency of interactions of 23 different ligands with certain amino acids of these receptors.

Success criteria set in docking analysis

In the current study, the lowest of all clusters in terms of the binding free energy was considered as the energetically most stable configuration and taken as reference (Morris and Lim-Wilby, 2008). The calculated inhibition constant (K_i) obtained with AutoDock 4.2.6 for each docked phytochemical were also represented.

Calculation of relative binding capacity index (RBCI) values

In this study, the relative binding capacity index (RBCI) was applied to statistically rank the activity potentials of phytochemicals by using binding free energy and inhibition constant values obtained from the docking analyses (Istifli et al., 2020). Using the RBCI, it is possible to compare statistically related data with different scientific meanings. If the ranking of the interactions of the ligands with proteins is performed only in light of one parameter (e.g. solely the binding free energy or inhibition constant), the phytochemicals can only be ordered in terms of their potential in this parameter. However, ranking based on only one of these parameters cannot represent the full activity potential of these molecules. The most common method used to calculate the interaction between the receptor and the ligand in multiple measurements is the 'central tendency', in which the components are ranked based on the average value of each component. However, since the units and scales of the data obtained from each parameter are different, it is not possible to obtain a universal value for all components.

If the values in each data set (binding free energy and inhibition constant) are converted to standard scores, it is possible to compare them with each other. In order to calculate the arithmetic mean values, first of all, binding free energy and inhibition constant of each phytochemical were used regardless of their units and raw values were obtained. These raw values calculated for each component were subtracted from the arithmetic mean and divided by standard deviation, and standard scores were obtained (see equation given below) (Sharma, 1996). RBCI values of each phytochemical were calculated by averaging these standard scores obtained separately for each protein target.

$$\text{Standard score} = \frac{(x-\mu)}{\sigma}$$

where 'x' is the raw data, 'μ' is the mean, and 'σ' is the standard deviation.

Although RBCI is a relative measure and does not represent the specific binding capacities of the components, it makes it possible to rank components reasonably based on their binding free energy and inhibition constant values. Therefore, it can be used as an integrated approach to evaluate the molecular interaction of the components, considering all parameters.

Molecular dynamics of top-ranked receptor-ligand complexes and molecular mechanics Poisson-Boltzmann surface area (MM/PBSA) calculations

The most favorable configurations obtained from the docking of receptor-ligand complexes (lowest binding free energy which means highest affinity), were used for the molecular dynamics simulations with the following procedure: the receptor coordinates files were converted from pdbqt format to pdb format using Babel (O'Boyle et al., 2011) and used as input geometry for molecular dynamics simulations using standard GROMACS (Abraham et al., 2015) tools, choosing the AMBER03 force field (Duan et al., 2003). The ligand coordinates files were modified using AutoDockTools (G. M. Morris et al., 2009), adding hydrogen atoms and converting to pdb files. These were submitted to the Acpype online server (Sousa da Silva & Vranken, 2012) to generate GROMACS topology files, using the parameters of the General Amber Force Field, GAFF (J. Wang, Wolf, Caldwell, Kollman, & Case, 2004) and AM1-BCC partial charges (Jakalian, Jack, & Bayly, 2002). The coordinates and topologies of ligands and receptors were then combined to construct the coordinates and topologies of the complexes. The complexes were then solvated using TIP3P water molecules (Jorgensen, Chandrasekhar, Madura, Impey, & Klein, 1983), a model suited to be used with AMBER Force Field, as well as sodium and chloride ions corresponding to physiological concentration, employing cubic simulation boxes with periodic boundary conditions. The van der Waals interactions were calculated directly until a 1.2 nm cutoff and the electrostatic interactions were calculated using the Particle Mesh Ewald (PME) method (Darden, York, & Pedersen, 1993; Essmann et al., 1995). The constructed systems were initially energetically minimized using the steepest descent algorithm and after the minimization, they were submitted to a 500 ps long simulation using position restraints for both receptor and ligand to allow the solvent and ions to relax without disturbing the complex geometry. After this phase, a sequence of three unrestricted molecular dynamics simulations with 5 ns each in temperatures of 200 K, 240 K, and 280 K was carried out, for the thermalization (heating) of the system. After these steps, 200 ns long production simulation runs, in the NPT ensemble, were carried out, employing a Nosé-Hoover thermostat (Hoover, 1985; Nosé, 1984) and a Parrinello-Rahman barostat (Parrinello & Rahman, 1981). Because of the minimization and thermalization procedures, the initial structures of the production phase of the molecular dynamics

simulations could deviate slightly from the final structures obtained from the docking. The trajectories were then analyzed to quantify the structural and thermodynamic stability of the complexes and also to identify the intermolecular interactions pattern. The time evolution of the pattern of interactions was also investigated using detailed qualitative visual analyses.

The intensity of the binding free energy between ligands and receptors was estimated using Molecular mechanics Poisson-Boltzmann surface area (MM/PBSA) binding free energy calculations (Baker et al., 2001; Homeyer and Gohlke, 2012). Sets of 200 configurations for each system were obtained as 1ns spaced snapshots, obtained directly from the molecular dynamics trajectories. The calculations were carried out using the g_mmpbsa GROMACS-compatible free energy program (Kumari et al., 2014) with a gridspace of 0.5 Å, salt concentration of 0.150 M, solute dielectric constant of 2 and employing the solvent accessible surface area (SASA) as estimate of the nonpolar solvation energy.

Drug-likeness and ADMET profile

Drug-likeness feature is a helpful concept in optimizing the properties of a bioactive molecule such as solubility, stability, bioavailability and distribution profile (Vistoli et al., 2008). In addition, the drug-likeness and ADMET profiles of potential hit compounds are very important in terms of reducing side effects in the pharmaceutical industry. Therefore, in the current study, web-based SwissADME and pkCSM tools were used to determine such effects of flavonoids analyzed (Daina et al., 2017, 2019; Delaney, 2004; Pires et al., 2015).

Supplementary Tables

Table S1. Relative binding capacity index (RBCI) values of flavonols*.

Compound	RBCI value
Robinin	–0.64
Gossypetin	–0.43
Pachypodol	–0.35
Fisetin	–0.35
Quercitrin	–0.34
3-Hydroxyflavone	–0.33
Rhamnazin	–0.31
Rhamnetin	–0.29
Kaempferide	–0.27
Morin	–0.23
Hyperoside	–0.23
Azaleatin	–0.18
Galangin	–0.18
Kaempferitrin	–0.16
Natsudaidain	–0.12
Astragalin	–0.07
Azalein	–0.07
Myricitrin	0.09
Xanthorhamnin	0.13
Amurensin	0.28
Icariin	0.30
Spiraeoside	0.50
Troxerutin	3.99

* The binding free energy and the inhibition constants of the ligands were taken into account when calculating the RBCI values.

Table S2. Molecular interactions between the flavonols and receptor binding domain (RBD) of the spike glycoprotein of 2019-nCoV.

No	Compound	Classical H-bond	Van der Waals	Nonclassical H-bond (C-H, Pi-Donor)	Hydrophobic interaction		Electrostatic	Miscellaneous (Lone pair/Pi-sulphur)
					p-p interaction	Mixed p/ Alkyl		
1	3-Hydroxyflavone	Gly496, Ser494[1]	Gln493[1], Tyr495, Phe497, Asn501[1], Tyr505[1]	-	Tyr453	Arg403	-	-
2	Azaleatin	Glu406, Ser494[1], Gln498, Asn501[1]	Ile418, Tyr449, Tyr495	Gly496	Tyr453, Tyr505[1]	-	Arg403	-
3	Fisetin	Gly502, Ser494[1], Gln498	Arg403, Tyr449, Tyr453, Tyr495, Gly496, Asn501[1], Tyr505[1]	-	-	-	-	-
4	Galangin	Gly496, Gln498, Gly502	Tyr495, Phe497, Asn501[1]	-	Tyr505[1]	Arg403	-	-
5	Gossypetin	Ser494[1], Gly496, Gln498, Tyr505[1]	Arg403, Tyr449, Tyr453, Tyr495, Phe497, Asn501[1]	Gln498	-	-	-	-
6	Kaempferide	Arg403, Ser494[1], Gln498	Glu406, Tyr449, Gln493[1], Tyr495, Gly496	Arg403	-	Tyr453	-	-
7	Morin	Glu406, Ser494[1], Gln498	Arg403, Tyr449, Tyr453, Tyr505[1]	Tyr495	-	-	-	-
8	Natsudaidain	Arg403, Gly496, Gln498	Tyr449, Tyr453, Gln493[1], Tyr495, Phe497	Arg403, Glu406, Ser494[1], Asn501[1]	-	-	-	-
9	Pachypodol	Arg403, Glu406, Gly496, Gln498	Tyr449, Tyr453, Ser494[1], Tyr495, Phe497, Asn501[1]	Gly496, Tyr505[1]	-	-	-	-

Table S2. (Continued).

10	Rhamnazin	Ser494[1], Gln498, Gly502	Arg403, Tyr453, Tyr495, Gly496, Phe497, Thr500, Asn501[1]	Tyr505[1]	Tyr505[1]	-	-	-
11	Rhamnetin	Arg403, Glu406, Tyr449, Tyr453, Gln493[1]	Ser494[1], Tyr495, Gln498	Gln498	-	-	-	-
12	Amurensin	Tyr449, Gln493[1], Gly496, Gln498, Gly502, Ser494[1], Tyr505[1]	Arg403, Tyr495, Phe497, Thr500, Gln506	-	-	-	-	-
13	Astragalin	Arg403, Gln493[1], Ser494[1], Tyr505[1]	Gln409, Lys417, Leu455[1], Tyr495, Gly496, Phe497, Asn501[1]	Arg403	Tyr453, Tyr505[1]		Arg403, Glu406	-
14	Azalein	Gln493[1], Ser494[1], Gly496, Gln498, Asn501[1]	Glu406, Tyr449, Tyr453, Tyr495, Gly502	Gly496	Tyr505[1]	-	Arg403	-
15	Hyperoside	Arg403, Glu406, Tyr449, Gln493[1], Gly496, Gln498	Leu455[1], Ser494[1], Phe497, Tyr505[1]	Tyr495, Gly496	-	-	-	Tyr453
16	Icariin	Tyr449, Gly496, Gln498, Tyr505[1]	Arg403, Lys417, Ile418, Leu455[1], Gln493[1], Ser494[1], Asn501[1]	Glu406, Gly496	Tyr453, Tyr505[1]	Tyr453, Tyr495	-	-
17	Kaempferitrin	Glu406, Ser494[1], Gly496	Leu455[1], Phe456, Tyr495, Gln498	Arg403, Lys417	Tyr453	Arg403, Lys417, Phe497, Tyr505[1]	Arg403	-
18	Myricitrin	Glu406, Ser494[1], Gly496, Tyr505[1]	Leu455[1], Tyr495, Asn501[1]	Arg403, Lys417	Tyr453	Lys417, Phe497, Tyr505[1]	-	-

Table S2. (Continued).

19	Quercitrin	Ser494[1], Gly496	Arg403, Tyr449, Tyr453, Gln493[1], Tyr495, Phe497, Gln498, Asn501[1], Tyr505[1]	-	-	-	-	Ser494[1]
20	Robinin	Tyr453, Gln493[1], Ser494[1], Gly496, Tyr505[1]	Asp405, Tyr449, Phe456, Tyr489, Phe490, Tyr495, Phe497, Asn5011	Ser494[1]	Tyr505[1]	Leu455[1]	Arg403	-
21	Spiraeoside	Arg403, Glu406, Tyr449, Gly496, Gln498, Asn501[1]	Lys417, Tyr495, Phe497	Arg403, Gln498	Tyr453, Tyr505[1]	Leu455[1]	Arg403	Tyr453
22	Troxerutin	-	-	-	-	-	-	-
23	Xanthorhamnin	Arg403, Gln493[1], Gly496, Tyr505[1], Glu406	Gln409, Tyr416, Tyr449, Tyr453, Ser494[1], Tyr495, Phe497, Gln498, Asn501[1]	Arg403, Glu406	-	Lys417, Leu455[1]	Glu406	-

[1]Amino acid residues involved in binding to ACE2 in the receptor binding motif (RBM) of 2019-nCoV (Leu455, Phe486, Gln493, Ser494, Asn501, and Tyr505).

Table S3. Molecular interactions between the flavonols and transmembrane protease, serine 2 (TMPRSS2).

No	Compound	Classical H-bond	Van der Waals	Nonclassical H-bond (C-H, Pi-Donor)	Hydrophobic interaction		Electrostatic	Miscellaneous (Lone pair/Pi-sulphur)
					p-p interaction	Mixed p/ Alkyl		
1	3-Hydroxyflavone	Thr387	Gly259, Ile381, Gly385, Glu388, Glu389, Asn398, Asn433, Ser436, Asp440, Cys465	Ala386	Thr387, Glu388	Ala466, Cys347	Thr387, Asp435, Ala466	-
2	Azaleatin	His279, Val280, Thr393, Ser394, Gln438	Cys281, His296[1], Gln317, Trp384, Glu395, Gly439, Ser441[1]	His279	-	Val280	His279, Thr393	-
3	Fisetin	His279, Val280, Thr393, Ser394, Gln438	Cys281, His296[1], Gln317, Trp384, Glu395, Gly439, Ser441[1]	His279	-	Val280	His279, Thr393	-
4	Galangin	Ala386, Asn433	Ile381, Glu388, Asn398, Ala400, Val434, Asp435, Ser436, Asp440, Cys465, Lys467	Ala386	Gly385, Ala386, Thr387, Glu388	Ala466, Cys347	Thr387, Ala466	-
5	Gossypetin	Asp435, Asn433, Cys465, Asp440	Gly259, Ile381, Gly385, Glu388, Glu389, Ala400, Val434, Ser436, Lys467	-	Thr387, Glu388	Cys437, Cys465, Ala466	Ala386, Thr387	-

Table S3. (Continued).

6	Kaempferide	His296[1], Ser441[1]	Val278, Val280, Ala294, Cys297, Trp384, Thr393, Ser394, Gln438, Gly439, Gly442	-	-	-	His279	Cys281
7	Morin	Val280, Ser441[1], Gly462	His279, Glu389, Gly439, Ser460, Gly464	His296[1], Trp461	-	-	-	-
8	Natsudaidain	Ser394, Gly439	Val278, Val280, Cys281, His296[1], Gln317, Trp384, Gly385, Thr393, Gln438, Ser441[1]	Gly439	-	-	His279	-
9	Pachypodol	Ser460	His296[1], Lys390, Ser436, Cys437, Gln438, Ser441[1], Trp461, Ser463, Gly464, Lys467	-	-	-	Glu389, Gly462	-
10	Rhamnazin	Ser460, Gly462, Glu389	His296[1], Ser436, Cys437, Gln438, Ser441[1], Trp461, Ser463, Gly464, Lys467	-	-	Lys390	Glu389	-
11	Rhamnetin	His279, Thr393, Gln438, Ser394	Cys281, His296[1], Trp384, Glu395, Gly439, Ser441[1]	His279	-	Val280	His279, Thr393	-

Table S3. (Continued).

12	Amurensin	Trp384, Thr393	Val278, His296[1], Leu302, Gln317, Glu389, Lys390, Ser394, Gly439, Trp461	-	-	Val280, Gln438	His279, Val280	-
13	Astragalin	Val280, Gln438	Cys281, Glu389, Thr393, Gly439, Ser441[1]	Val280, Lys390, Gln438	-	Val278	-	-
14	Azalein	Glu389, Gly464	Lys390, Tyr416, Gln438, Ser463, Cys465	Ser441[1]	-	-	Trp461, Gly462	-
15	Hyperoside	Glu389, Gly462	Lys390, Tyr416, Cys437, Gly439, Ser441[1], Ser460, Lys467	His296[1], Trp461	-	Ser463	Glu389, Gly462	-
16	Icariin	-	-	-	-	-	-	-
17	Kaempferitrin	-	-	-	-	-	-	-
18	Myricitrin	Glu389, Ser460, Gly462	His296[1], Lys390, Tyr416, Ser436, Cys437, Ser441[1], Ser463, Cys465, Lys467	Trp461, Gly464	-	-	Glu389, Gly462	-
19	Quercitrin	Val280, Cys281, Gln438, Ser460, Gly462, Gly439, Ser441[1]	Ala294, Val278, Trp308, Thr393, Gly442, Trp461, Gly464	Val280, His296[1]	His296[1]	Val280, Cys281	Val280, His296[1]	Cys297

Table S3. (Continued).

20	Robinin	His279, Gln317, Lys340, Gly439	Val278, Val280, Cys281, Gly282, Cys297, Glu299, Tyr337, Thr341, Lys342, Trp384, Gly385, Thr393, Asp440, Ser441[1]	His296[1]	His296[1]	Lys340	-	-
21	Spiraeoside	Cys437, Gln438, Gly439, Ser441[1], Ser460, Gly462	Val278, His279, Glu389, Lys390, Thr393, Thr459, Trp461, Ser463, Gly464	Val280, His296[1], Gln438	-	-	Val280	-
22	Troxerutin	-	-	-	-	-	-	-
23	Xanthorhamnin	-	-	-	-	-	-	-

[1]The active amino acid residues of transmembrane protease, serine 2 (TMPRSS2) (His296, Asp345, Ser441).

Table S4. Molecular interactions between the flavonols and cathepsin B (CatB).

No	Compound	Classical H-bond	Van der Waals	Nonclassical H-bond (C-H, Pi-Donor)	Hydrophobic interaction		Electrostatic	Miscellaneous (Lone pair/Pi-sulphur)
					p-p interaction	Mixed p/ Alkyl		
1	3-Hydroxyflavone	Cys26[1], His111[1], Gly121	Gln23[1], Gly24[1], Ser25, Gly27[1], Cys29[1], Glu109, His110[1], Thr120, Glu122, His199[1], Trp221[1]	-	His111[1]	Cys119	His111[1]	-
2	Azaleatin	Gln23[1], Gly24[1], His111[1], Cys119, Gly121	Ser25, Gly27[1], Cys29[1], Glu109, His110[1], Pro118, Thr120, Val176, Gly198, His199[1]	-	His111[1], Gly121	Cys119	His111[1]	-
3	Fisetin	Gln23[1], Gly24[1], Cys26[1], His111[1], Cys119, Gly121	Ser25, Gly27[1], Cys29[1], Glu109, Pro118, Thr120, Val176	His110[1], His199[1]	His110[1], His111[1], Trp221[1]	-	His111[1]	Cys119
4	Galangin	Cys26[1], His111[1], Gly121	Gln23[1], Gly24[1], Ser25, Gly27[1], Ser28[1], Cys29[1], Glu109, Thr120, Glu122, Val176	His110[1], His199[1]	His110[1], His111[1], Trp221[1]	Cys119	His111[1]	-
5	Gossypetin	Gln23[1], Cys26[1], His111[1], Cys119, Gly121	Gly24[1], Ser25, Gly27[1], Ser28[1], Cys29[1], Glu109, His110[1], Pro118, Thr120, Glu122, Val176, Leu181, Trp221[1]	Gly27[1]	His111[1]	Cys119	His111[1]	-

Table S4. (Continued).

6	Kaempferide	Cys26[1], His111[1], Gly121	Gln23[1], Gly24[1], Ser25, Ser28[1], Cys29[1], Glu109, His110[1], Pro118, Glu122, Val176, Gly198, His199[1]	Gly27[1]	His111[1], Trp221[1]	Cys119	His111[1]	-
7	Morin	Cys26[1], Glu109, His111[1], Gly121	Gln23[1], Gly24[1], Ser25, Ser28[1], Cys29[1], Pro118, Thr120, Glu122, Val176, His199[1], Trp221[1]	Gly27[1]	His110[1], His111[1]	Cys119	His111[1]	Cys119
8	Natsudaidain	Gln23[1], Gly24[1], His111[1], His199[1]	Ser25, Gly27[1], Ser28[1], Cys29[1], Glu109, His110[1], Pro118, Thr120, Gly121, Val176, Met196	Gly198	His111[1], Trp221[1]	Cys119	His111[1]	-
9	Pachypodol	His111[1], Cys119, Gly121	Gln23[1], Gly24[1], Ser25, Cys26[1], Cys29[1], Glu109, His110[1], Pro118, Thr120, Val176, Met196, Gly197	Gly121, Gly198, His199[1]	His111[1], Trp221[1]	His111[1], Cys119	-	-
10	Rhamnazin	Gln23[1], Gly24[1], Cys26[1], His111[1], Gly121	Gly27[1], Glu109, Pro118, Thr120, Glu122, Val176, Trp221[1]	Ser25, Cys119, His199[1]	His110[1], His111[1]	Cys119	His111[1]	Cys119

Table S4. (Continued).

11	Rhamnetin	Cys26[1], Glu109, His111[1], Cys119, Gly121	Gln23[1], Gly24[1], Ser25, Gly27[1], Ser28[1], Cys29[1], His110[1], Pro118, Thr120, Glu122, Val176, Gly198, His199[1]	-	His111[1], Trp221[1]	Cys119	-	-
12	Amurensin	Gln23[1], Gly24[1], Cys26[1], Glu109, Glu122, Met196, Gly198	Ser25, Ser28[1], Asn72, Gly73[1], His110[1], Pro118, Gly121, Val176, Leu181, Gly197, His199[1], Trp221[1]	Gly27[1], Glu122	His111[1]	Cys119	His111[1], Glu122	Cys119
13	Astragalin	Gln23[1], Gly24[1], His110[1], His111[1], Gly198, Trp221[1]	Ser25, Gly27[1], Ser28[1], Cys119, Gly121, Val176, Gly197	Cys26[1], His199[1]	-	Cys29[1], Met196	Glu122, His111[1]	-
14	Azalein	Gly24[1], Gly74[1], Gly121, Glu122, Met196, Gly198	Gln23[1], Ser25, Gly73[1], His110[1], Cys119, Gly197, His199[1], Trp221[1]	Gly27[1], Cys29[1], Trp30[1]	-	Cys26[1], Gly27[1]	-	-
15	Hyperoside	Gly121, Glu122, Met196	Gln23[1], Gly24[1], Ser25, Cys26[1], Gly27[1], Trp30[1], Asn72, Gly73[1], Gly74[1], His110[1], His111[1], Thr120, Val176, His199[1], Trp221[1]	Gly197, Gly198	-	Cys119	-	Cys29[1]

Table S4. (Continued).

16	Icariin	Gly24[1], Asn72, Gly121, Glu122	Gln23[1], Ser25, Cys26[1], Gly27[1], Trp30[1], Gly73[1], Gly74[1], Pro76, His110[1], His111[1], Cys119, Thr120, Phe180, Ala200	Cys29[1]	His199[1], Trp221[1]	Val176	-	Cys29[1]
17	Kaempferitrin	Gly24[1], Gly27[1], Trp30[1], Gly74[1], His110[1], His111[1], Gly121, Trp221[1]	Gln23[1], Ser25, Cys26[1], Ser28[1], Asn72, Gly73[1], Glu109, Glu122, Leu181, Gly198	His199[1]	His111[1]	His110[1], His111[1], Cys119, Met196	His111[1]	Cys29[1]
18	Myricitrin	Gln23[1], Gly24[1], Gly27[1], Gly74[1], His110[1], His111[1], Glu122, Met196, Gly198	Ser25, Cys26[1], Ser28[1], Trp30[1], Gly73[1], Gly121, Gly197, His199[1], Trp221[1]	Cys29[1]	-	Cys29[1], Met196	-	-
19	Quercitrin	Gln23[1], Gly24[1], Gly27[1], Gly74[1], His111[1], Gly121, Gly198, Trp221[1]	Ser25, Ser28[1], Trp30[1], Gly73[1], His110[1], Cys119, Val176, Gly197	Gly27[1], Cys29[1], His199[1]	-	Cys29[1], His111[1], Leu181, Met196	Glu122	-
20	Robinin	Gln23[1], Cys26[1], Cys29[1], Gly74[1], Glu109, Cys119, Glu122, Gly197	Gly24[1], Ser25, Gly27[1], Ser28[1], Trp30[1], Gly73[1], Tyr75, Pro76, His110[1], Pro118, Thr120, Met196, Gly198, His199[1], Trp221[1]	-	-	His111[1], Val176	-	Cys119

Table S4. (Continued).

21	Spiraeoside	Gly24[1], Cys26[1], Gly27[1], Gly74[1], Gly198	Gln23[1], Ser25, Ser28[1], Trp30[1], Pro76, His110[1], His111[1], Cys119, Gly121, Glu122, Ala173, Gly197, Ala200, Trp221[1]	Gly27[1], Cys29[1], Gly73[1]	-	Cys29[1]	-	-
22	Troxerutin	Gly74[1], His110[1], Met196, Gly198, His199[1], Trp221[1]	Gln23[1], Gly24[1], Cys26[1], Trp30[1], Thr120, Gly121, Glu122, Val176, Leu181, Gly197, Ala200	Ser25, Gly27[1], Gly73[1], His111[1], His199[1]	-	Cys29[1]	Cys119	-
23	Xanthorhamnin	Gln23[1], Gly24[1], Cys26[1], Cys29[1], Gly74[1], His111[1], Glu122, Gly198, His199[1], Trp221[1]	Ser25, Gly27[1], Trp30[1], Cys71, Asn72, Pro76, Gly121, Leu181, Gly197, Glu245	Gly73[1]	-	His110[1], His111[1], Cys119, Ala173, Val176, Met196 Ala200, Trp221[1]	-	-

[1]The active amino acid residues of cathepsin B (CatB) (Gln23, Gly24, Cys26, Gly27, Ser28, Cys29, Trp30, Gly73, Gly74, His110, His111, His199, Trp221).

Table S5. Molecular interactions between the flavonols and cathepsin L (CatL).

No	Compound	Classical H-bond	Van der Waals	Nonclassical H-bond (C-H, Pi-Donor)	Hydrophobic interaction		Electrostatic	Miscellaneous (Lone pair/Pi-sulphur)
					p-p interaction	Mixed p/ Alkyl		
1	3-Hydroxyflavone	Asp71	Asp114, Ile115, Ser213, Ala215, Ser216	-	-	Leu69[1], Lys117, Ala214	Lys117	Met70[1]
2	Azaleatin	Met70[1], Asp71, Asp114, Glu159, Met161[1]	Gly68[1], Asp160, Ser216	Leu69[1]	-	Leu69[1], Ala135[1], Met161[1], Ala214	-	Met70[1]
3	Fisetin	Asp114, Ile115	Met70[1], Tyr72, Phe112, Pro116, Ala212, Ser213, Ala215	Asp71	-	Leu69[1], Asp114, Ile115, Lys117, Ala214	Asp71, Asp114, Lys117	-
4	Galangin	Ser216	Leu69[1], Tyr72, Phe74, Ile115, Ser133, Ala215	-	-	Lys117, Ala214	Asp71, Asp114, Lys117	Met70[1]
5	Gossypetin	Asp71, Asp114, Ile115, Ala215, Ser216	Pro116, Met161[1], Ser213	-	-	Leu69[1], Ala135[1], Ala214	Asp114, Lys117	Met70[1]
6	Kaempferide	Met70[1], Asp71, Asp114, Ile115	Gly68[1], Phe112, Pro116, Ala135[1], Ser213, Ala215, Ser216	-	-	Leu69[1], Asp114, Ile115, Ala214	Asp114, Lys117	Met70[1]
7	Morin	Ile115, Ser133, Ala215, Ser216	Leu69[1], Tyr72, Phe74, Pro116, Val134, Ser213	-	-	Lys117, Ala214	Asp71, Asp114, Lys117	Met70[1]
8	Natsudaidain	Gly68[1], Met70[1], Asp71, Asp114, Met161[1]	Trp26[1], Tyr72, Phe112, Asp162[1], His163, Gly164, Ser216	-	-	Leu69[1], Ala135[1], Ala214	Asp71, Asp114	Met70[1]

Table S5. (Continued).

9	Pachypodol	Met70[1], Asp114, Lys117,	Trp26[1], Gly68[1], Phe112, Met161[1], Gly164, Ser216	-	-	Leu69[1], Ala135[1], Ala214	Asp71, Asp114	Met70[1]
10	Rhamnazin	Gly23[1], Met70[1], Met161[1]	Ser24[1], Trp26[1], Asn66[1], Gly67[1], Asp71, His163, Ser216	Gly68[1], Asp162[1]	-	Cys25[1], Leu69[1], Met70[1], Ala135[1], Ala214	-	-
11	Rhamnetin	Gly23[1], Cys25[1], Trp26[1], Met70[1], Met161[1]	Ser24[1], Asn66[1], Gly67[1], Asp71, Asp162[1]	Gly68[1]	-	Cys25[1], Leu69[1], Met70[1], Ala135[1], Ala214	-	-
12	Amurensin	Met70[1], Glu159, Asp160, Asp162[1]	Cys25[1], Trp26[1], Asp71, His163, Gly164, Ser213	-	-	Leu69[1], Ala135[1], Asp160 Met161[1], Ala214	-	Met70[1], Met161[1]
13	Astragalin	Asp114, Ile115, Ser216	Leu69[1], Tyr72, Phe74, Phe112, Pro116, Ser133, Ala215	-	-	Met70[1], Lys117, Ala214	Asp71, Asp114, Lys117	-
14	Azalein	Cys25[1], Gly68[1], Met70[1], Asp71, Asp114, Met161[1], Asp162[1], Gly164	Ser133, Glu159, Asp160, His163, Ser216	Ala214	-	Cys25[1], Trp26[1], Leu69[1], Met70[1], Ala135[1], Ala214	-	Met70[1], Met161[1]
15	Hyperoside	Gly23[1], Gly61[1], Asn66[1], Gly68[1], Met161[1]	Ser24[1], Cys25[1], Trp26[1], Asn62, Glu63, Cys65, Tyr72, Asp160, Ala214	Asp162[1]	Leu69[1], Ala135[1]	Gly67[1], Gly68[1], Leu69[1]	-	-
16	Icariin	Asn66[1], Gly68[1], Met70[1], Asp71, Asp114, Asp162[1], Ala214, Ser216	Trp26[1], Gly67[1], Ser133, Asp160, His163, Gly164, Ala215	-	-	Leu69[1], Ala135[1], Met161[1], Ala214	-	Met70[1]

Table S5. (Continued).

17	Kaempferitrin	Asn66[1], Gly68[1], Asp71, Asp114	Gly23[1], Tyr72, Phe74, Lys117, Ser133, Met161[1], Asp162[1], Gly164, Ala215	Gly67[1], Asp71	-	Cys25[1], Trp26[1], Leu69[1], Ala135[1], Ala214	-	Met70[1]
18	Myricitrin	Cys25[1], Asp71, Asp114, Lys117, Met161[1], Ser213, Ser216	Trp26[1], Gly68[1], Phe74, Ser133, Glu159, His163, Ala215	Asp162[1]		Leu69[1], Met70[1], Ala135[1], Met161[1], Ala214		Cys25[1], Met70[1]
19	Quercitrin	Gly68[1], Met70[1], Asp71, Asp114, Glu159, Met161[1]	Cys25[1], Trp26[1], Gly67[1], Ile136, Asp162[1], His163, Gly164, Ser216	-	Asp160, Met161[1]	Leu69[1], Ala135[1], Met161[1], Ala214	-	-
20	Robinin	Gly68[1], Asp114, Ser133, Met161[1], Asp162[1], Ser216	Gly23[1], Gly67[1], Tyr72, Phe74, Phe112, Val134, His163, Gly164	Gly68[1]	-	Cys25[1], Trp26[1], Leu69[1], Ala214	Asp71	Met70[1]
21	Spiraeoside	Gly23[1], Asp71, Asp114, Met161[1]	Cys25[1], Trp26[1], Gly67[1], Gly68[1], Ser133, Asp162[1], Ser216	-	Asn66[1], Gly67[1]	Leu69[1], Ala135[1], Ala214	-	Met70[1]
22	Troxerutin	Gly23[1], Met70[1], Asp71, Tyr72	Trp26[1], Gly61[1], Cys65, Asn66[1], Gly67[1], Asp114, Met161[1], His163, Gly164, Ala214, Ser216	Glu63, Gly68[1], Asp71	-	Cys25[1], Leu69[1]	-	Gly68[1]

Table S5. (Continued).

23	Xanthorhamnin	Cys25[1], Glu63, Gly68[1], Asp71, Glu159, Met161[1]	Trp26[1], Gly61[1], Asn62, Gly67[1], Ile136, Asp160, Asp162[1], His163, Gly164, Ser216	Gly68[1], Asp71	-	Leu69[1], Tyr72, Ala135[1], Met161[1], Ala214	-	Met70[1]

[1]The active amino acid residues of cathepsin L (CatL) (Gln19, Gly20, Gln21, Cys22, Gly23, Ser24, Cys25, Trp26, Gly61, Asn66, Gly67, Gly68, Leu69, Met70, Ala135, Met161, Asp162, Trp189).

Supplementary Figures

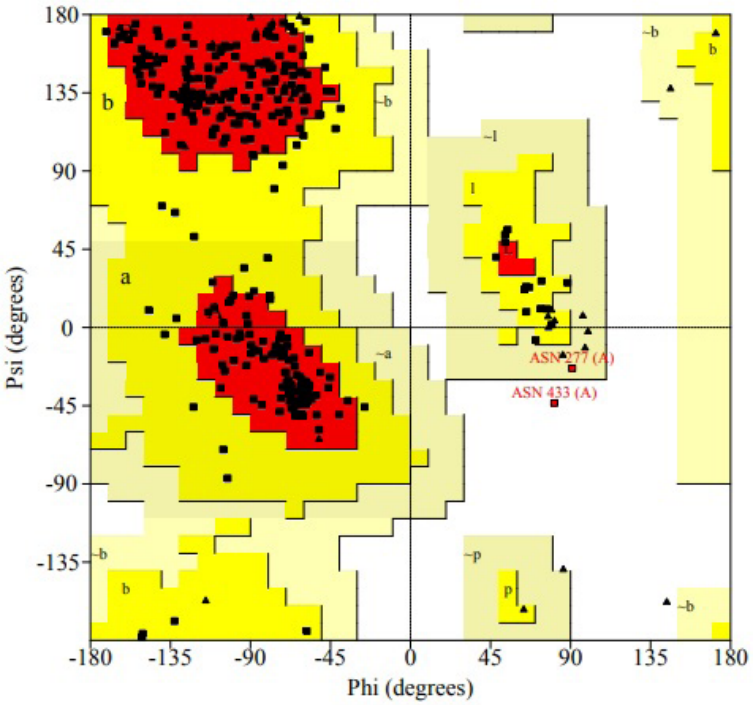

Figure S1. Ramachandran plot of TMPRSS2 model. 84.6% of the residues are in the core (red) region, 14.7% of the residues are in the allowed regions (yellow), 0.3% of the residues are in the generously allowed regions (grey), and 0.3% of the residues are in the disallowed regions (white) (https://saves.mbi.ucla.edu/Jobs/708717/pc/saves.sum).

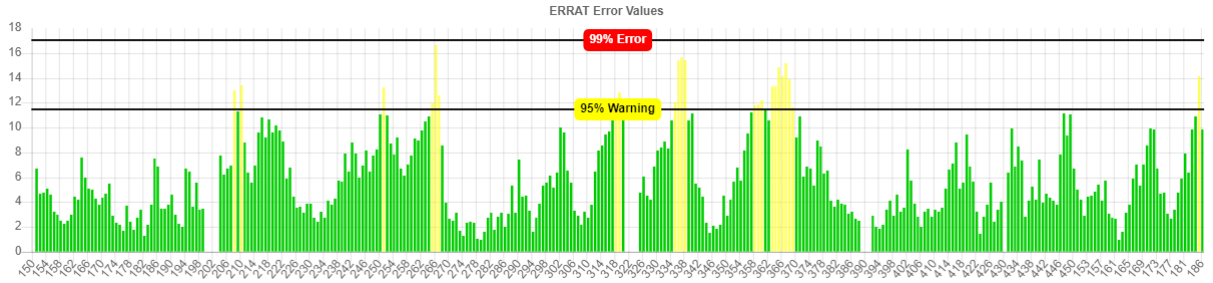

Figure S2. ERRAT error values for TMPRSS2 model.
(Protein regions show misfolding at 95% confidence level were indicated with yellow bars. Green bars, on the other hand, point to regions that show correct folding).

Gln506	0	0	0	0	0	0	0	0	0	0	0	1	0	0	0	0	0	0	0	0	0	0	0
Tyr505[1]	1	1	1	1	1	0	1	0	1	2	0	1	2	1	1	2	1	2	1	2	1	0	1
Gly502	0	0	1	1	0	0	0	0	0	1	0	1	0	1	0	0	0	0	0	0	0	0	0
Asn501[1]	1	1	1	1	1	0	0	1	1	1	0	0	1	1	0	1	0	1	1	1	1	0	1
Thr500	0	0	0	0	0	0	0	0	0	1	0	1	0	0	0	0	0	0	0	0	0	0	0
Gln498	0	1	1	1	2	1	1	1	1	1	2	1	0	1	1	1	1	0	1	0	2	0	1
Phe497	1	0	0	1	1	0	0	1	1	1	0	1	1	0	1	0	1	1	1	1	1	0	1
Gly496	1	1	1	1	1	1	0	1	2	1	0	1	1	2	2	2	1	1	1	1	1	0	1
Tyr495	1	1	1	1	1	1	1	1	1	1	1	1	1	1	1	1	1	1	1	1	1	0	1
Ser494[1]	1	1	1	0	1	1	1	1	1	1	1	1	1	1	1	1	1	1	2	2	0	0	1
Gln493[1]	1	0	0	0	0	1	0	1	0	0	1	1	1	1	1	1	0	0	1	1	0	0	1
Phe490	0	0	0	0	0	0	0	0	0	0	0	0	0	0	0	0	0	0	0	1	0	0	0
Tyr489	0	0	0	0	0	0	0	0	0	0	0	0	0	0	0	0	0	0	0	1	0	0	0
Phe486[1]	0	0	0	0	0	0	0	0	0	0	0	0	0	0	0	0	0	0	0	0	0	0	0
Phe456	0	0	0	0	0	0	0	0	0	0	0	0	0	0	0	0	1	0	0	1	0	0	0
Leu455[1]	0	0	0	0	0	0	0	0	0	0	0	0	1	0	1	0	1	1	0	1	1	0	1
Tyr453	1	1	1	0	1	1	1	1	1	1	1	0	1	1	1	2	1	1	1	1	2	0	1
Tyr449	0	1	1	0	1	1	1	1	1	0	1	1	0	1	1	1	0	0	1	1	1	0	1
Ile418	0	1	0	0	0	0	0	0	0	0	0	0	0	0	0	1	0	0	0	0	0	0	0
Lys417	0	0	0	0	0	0	0	0	0	0	0	0	1	0	0	1	2	2	0	0	1	0	1
Tyr416	0	0	0	0	0	0	0	0	0	0	0	0	0	0	0	0	0	0	0	0	0	0	1
Gln409	0	0	0	0	0	0	0	0	0	0	0	0	1	0	0	0	0	0	0	0	0	0	1
Glu406	0	1	0	0	0	1	1	1	1	0	1	0	1	1	1	1	1	1	0	0	1	0	3
Asp405	0	0	0	0	0	0	0	0	0	0	0	0	0	0	0	0	0	0	0	1	0	0	0
Arg403	1	1	1	1	1	2	1	2	1	1	1	1	3	1	1	1	3	1	1	1	3	0	2
	1	2	3	4	5	6	7	8	9	10	11	12	13	14	15	16	17	18	19	20	21	22	23

Figure S3. Heatmap of flavonol/RBM of the spike glycoprotein of 2019-nCoV interaction. Heatmaps are built on the logic of how many times each ligand interacts with each residue (regardless of bond type).

Lys467	0	0	0	1	1	0	0	0	1	1	0	0	0	0	1	0	0	1	0	0	0	0	0
Ala466	2	0	0	2	1	0	0	0	0	0	0	0	0	0	0	0	0	0	0	0	0	0	0
Cys465	1	0	0	1	2	0	0	0	0	0	0	0	0	1	0	0	0	1	0	0	0	0	0
Gly464	0	0	0	0	0	0	1	0	1	1	0	0	0	1	0	0	0	1	1	0	1	0	0
Ser463	0	0	0	0	0	0	0	0	1	1	0	0	0	1	1	0	0	1	0	0	1	0	0
Gly462	0	0	0	0	0	0	1	0	1	1	0	0	0	1	2	0	0	2	1	0	1	0	0
Trp461	0	0	0	0	0	0	1	0	1	1	0	1	0	1	1	0	0	1	1	0	1	0	0
Ser460	0	0	0	0	0	0	1	0	1	1	0	0	0	0	1	0	0	1	1	0	1	0	0
Thr459	0	0	0	0	0	0	0	0	0	0	0	0	0	0	0	0	0	0	0	0	1	0	0
Gly442	0	0	0	0	0	1	0	0	0	0	0	0	0	0	0	0	0	0	1	0	0	0	0
Ser441[1]	0	1	1	0	0	1	1	1	1	1	1	0	1	1	1	0	0	1	1	0	1	0	0
Asp440	1	0	0	1	1	0	0	0	0	0	0	0	0	0	0	0	0	0	0	0	0	0	0
Gly439	0	1	1	0	0	1	1	2	0	0	1	1	1	0	1	0	0	0	1	0	1	0	0
Gln438	0	1	1	0	0	1	0	1	1	1	1	1	2	1	0	0	0	0	1	0	2	0	0
Cys437	0	0	0	0	1	0	0	0	1	1	0	0	0	0	1	0	0	1	0	0	1	0	0
Ser436	1	0	0	1	1	0	0	0	1	1	0	0	0	0	0	0	0	1	0	0	0	0	0
Asp435	0	0	0	1	1	0	0	0	0	0	0	0	0	0	0	0	0	0	0	0	0	0	0
Val434	0	0	0	1	1	0	0	0	0	0	0	0	0	0	0	0	0	0	0	0	0	0	0
Asn433	1	0	0	1	1	0	0	0	0	0	0	0	0	0	0	0	0	0	0	0	0	0	0
Tyr416	0	0	0	0	0	0	0	0	0	0	0	0	0	1	1	0	0	1	0	0	0	0	0
Ala400	0	0	0	1	1	0	0	0	0	0	0	0	0	0	0	0	0	0	0	0	0	0	0
Asn398	1	0	0	1	0	0	0	0	0	0	0	0	0	0	0	0	0	0	0	0	0	0	0
Glu395	0	1	1	0	0	0	0	0	0	0	1	0	0	0	0	0	0	0	0	0	0	0	0
Ser394	0	1	1	0	0	1	0	1	0	0	1	1	0	0	0	0	0	0	0	0	0	0	0
Thr393	0	2	2	0	0	1	0	1	0	0	2	1	1	0	0	0	0	0	1	0	1	0	0
Lys390	0	0	0	0	0	0	0	0	1	1	0	1	1	1	1	0	0	1	0	0	1	0	0
Glu389	1	0	0	0	1	0	1	0	1	2	0	1	1	1	2	0	0	2	0	0	1	0	0
Glu388	2	0	0	2	2	0	0	0	0	0	0	0	0	0	0	0	0	0	0	0	0	0	0
Thr387	3	0	0	2	2	0	0	0	0	0	0	0	0	0	0	0	0	0	0	0	0	0	0
Ala386	1	0	0	3	1	0	0	0	0	0	0	0	0	0	0	0	0	0	0	0	0	0	0
Gly385	1	0	0	1	1	0	0	1	0	0	0	0	0	0	0	0	0	0	0	0	0	0	0
Trp384	0	1	1	0	0	1	0	1	0	0	1	1	0	0	0	0	0	0	0	0	0	0	0
Ile381	1	0	0	1	1	0	0	0	0	0	0	0	0	0	0	0	0	0	0	0	0	0	0
Cys347	1	0	0	1	0	0	0	0	0	0	0	0	0	0	0	0	0	0	0	0	0	0	0
Asp345[1]	1	0	0	0	0	0	0	0	0	0	0	0	0	0	0	0	0	0	0	0	0	0	0
Gln317	0	1	1	0	0	0	0	1	0	0	0	1	0	0	0	0	0	0	0	0	0	0	0
Trp308	0	0	0	0	0	0	0	0	0	0	0	0	0	0	0	0	0	0	1	0	0	0	0
Leu302	0	0	0	0	0	0	0	0	0	0	0	1	0	0	0	0	0	0	0	0	0	0	0
Cys297	0	0	0	0	0	1	0	0	0	0	0	0	0	0	0	0	0	0	1	0	0	0	0
His296[1]	0	1	1	0	0	1	1	1	1	1	1	1	0	0	1	0	0	1	3	0	1	0	0
Ala294	0	0	0	0	0	1	0	0	0	0	0	0	0	0	0	0	0	0	1	0	0	0	0
Cys281	0	1	1	0	0	1	0	1	0	0	1	0	1	0	0	0	0	0	2	0	0	0	0
Val280	0	2	2	0	0	1	1	1	0	0	1	2	2	0	0	0	0	0	4	0	2	0	0
His279	0	3	3	0	0	1	1	1	0	0	3	1	0	0	0	0	0	0	0	0	1	0	0
Val278	0	0	0	0	0	1	0	1	0	0	0	1	1	0	0	0	0	0	1	0	1	0	0
Gly259	1	0	0	0	1	0	0	0	0	0	0	0	0	0	0	0	0	0	0	0	0	0	0
	1	2	3	4	5	6	7	8	9	10	11	12	13	14	15	16	17	18	19	20	21	22	23

Figure S4. Heatmap of flavonol/TMPRSS2 interaction. Heatmaps are built on the logic of how many times each ligand interacts with each residue (regardless of bond type).

Glu245	0	0	0	0	0	0	0	0	0	0	0	0	0	0	0	0	0	0	0	0	0	0	1
Trp221[1]	1	0	1	1	1	1	1	1	1	1	1	1	1	1	1	1	1	1	1	1	1	1	2
Ala200	0	0	0	0	0	0	0	0	0	0	0	0	0	0	0	1	0	0	0	0	1	1	1
His199[1]	1	1	1	1	0	1	1	1	1	1	1	1	1	1	1	1	1	1	1	1	0	2	1
Gly198	0	1	0	0	0	1	0	1	1	0	1	1	1	1	1	0	1	1	1	1	1	1	1
Gly197	0	0	0	0	0	0	0	0	1	0	0	1	1	1	1	0	0	1	1	1	1	1	1
Met196	0	0	0	0	0	0	0	1	1	0	0	1	1	1	1	0	1	2	1	1	0	1	1
Leu181	0	0	0	0	1	0	0	0	0	0	0	1	0	0	0	0	1	0	1	0	0	1	1
Phe180	0	0	0	0	0	0	0	0	0	0	0	0	0	0	0	1	0	0	0	0	0	0	0
Val176	0	1	1	1	1	1	1	1	1	1	1	1	1	0	1	1	0	0	1	1	0	1	1
Ala173	0	0	0	0	0	0	0	0	0	0	0	0	0	0	0	0	0	0	0	0	1	0	1
Glu122	1	0	0	1	1	1	1	0	0	1	1	3	1	1	1	1	1	1	1	1	1	1	1
Gly121	1	2	1	1	1	1	1	1	2	1	1	1	1	1	1	1	1	1	1	0	1	1	1
Thr120	1	1	1	1	1	0	1	1	1	1	1	0	0	0	1	1	0	0	0	1	0	1	0
Cys119	1	2	2	1	2	1	2	1	2	3	2	2	1	1	1	1	1	0	1	2	1	1	1
Pro118	0	1	1	0	1	1	1	1	1	1	1	1	0	0	0	0	0	0	0	1	0	0	0
His111[1]	3	1	3	4	3	3	3	3	3	3	2	2	2	0	1	1	4	1	2	1	1	1	2
His110[1]	1	1	2	2	1	1	1	1	1	1	1	1	1	1	1	1	2	1	1	1	1	1	1
Glu109	1	1	1	1	1	1	1	1	1	1	1	1	0	0	0	0	1	0	0	1	0	0	0
Pro76	0	0	0	0	0	0	0	0	0	0	0	0	0	0	0	1	0	0	0	1	1	0	1
Tyr75	0	0	0	0	0	0	0	0	0	0	0	0	0	0	0	0	0	0	0	1	0	0	0
Gly74[1]	0	0	0	0	0	0	0	0	0	0	0	0	0	1	1	1	1	1	1	1	1	1	1
Gly73[1]	0	0	0	0	0	0	0	0	0	0	0	1	0	1	1	1	1	1	1	1	1	1	1
Asn72	0	0	0	0	0	0	0	0	0	0	0	1	0	0	1	1	1	0	0	0	0	0	1
Cys71	0	0	0	0	0	0	0	0	0	0	0	0	0	0	0	0	0	0	0	0	0	0	1
Trp30[1]	0	0	0	0	0	0	0	0	0	0	0	0	0	1	1	1	1	1	1	1	1	1	1
Cys29[1]	1	1	1	1	1	1	1	1	1	0	1	0	1	1	1	2	1	2	2	1	2	1	1
Ser28[1]	0	0	0	1	1	1	1	1	0	0	1	1	1	0	0	0	1	1	1	1	1	0	0
Gly27[1]	1	1	1	1	2	1	1	1	0	1	1	1	1	2	1	1	1	1	2	1	2	1	1
Cys26[1]	1	0	1	1	1	1	1	0	1	1	1	1	1	1	1	1	1	1	0	1	1	1	1
Ser25	1	1	1	1	1	1	1	1	1	1	1	1	1	1	1	1	1	1	1	1	1	1	1
Gly24[1]	1	1	1	1	1	1	1	1	1	1	1	1	1	1	1	1	1	1	1	1	1	1	1
Gln23[1]	1	1	1	1	1	1	1	1	1	1	1	1	1	1	1	1	1	1	1	1	1	1	1
	1	2	3	4	5	6	7	8	9	10	11	12	13	14	15	16	17	18	19	20	21	22	23

Figure S5. Heatmap of flavonol/CatB interaction. Heatmaps are built on the logic of how many times each ligand interacts with each residue (regardless of bond type).

Ser216	1	1	0	1	1	1	1	1	1	1	0	0	1	1	0	1	0	1	1	1	1	1	1
Ala215	1	0	1	1	1	1	1	0	0	0	0	0	1	0	0	1	1	1	0	0	0	0	0
Ala214	1	1	1	1	1	1	1	1	1	1	1	1	1	2	1	2	1	1	1	1	1	1	1
Ser213	1	0	1	0	1	1	1	0	0	0	0	1	0	0	0	0	0	1	0	0	0	0	0
Ala212	0	0	1	0	0	0	0	0	0	0	0	0	0	0	0	0	0	0	0	0	0	0	0
Trp189[1]	0	0	0	0	0	0	0	0	0	0	0	0	0	0	0	0	0	0	0	0	0	0	0
Gly164	0	0	0	0	0	0	0	1	1	0	0	1	0	1	0	1	1	0	1	1	0	1	1
His163	0	0	0	0	0	0	0	1	0	1	0	1	0	1	0	1	0	1	1	1	0	1	1
Asp162[1]	0	0	0	0	0	0	0	1	0	1	1	1	0	1	1	1	1	1	1	1	0	1	
Met161[1]	0	2	0	0	1	0	0	1	1	1	1	2	0	2	1	1	1	2	3	1	1	1	2
Asp160	0	1	0	0	0	0	0	0	0	0	0	2	0	1	1	1	0	0	1	0	0	0	1
Glu159	0	1	0	0	0	0	0	0	0	0	0	1	0	1	0	0	0	1	1	0	0	0	1
Ile136	0	0	0	0	0	0	0	0	0	0	0	0	0	0	0	0	0	0	1	0	0	0	1
Ala135[1]	0	1	0	0	1	1	0	1	1	1	1	1	0	1	1	1	1	1	1	0	1	0	1
Val134	0	0	0	0	0	0	1	0	0	0	0	0	0	0	0	0	0	0	0	1	0	0	0
Ser133	0	0	0	1	0	0	1	0	0	0	0	0	1	1	0	1	1	1	0	1	1	0	0
Lys117	2	0	2	2	1	1	2	0	1	0	0	0	2	0	0	0	1	1	0	0	0	0	0
Pro116	0	0	1	0	1	1	1	0	0	0	0	0	1	0	0	0	0	0	0	0	0	0	0
Ile115	1	0	2	1	1	3	1	0	0	0	0	0	1	0	0	0	0	0	0	0	0	0	0
Asp114	1	1	3	1	2	2	1	2	2	0	0	0	2	1	0	1	1	1	1	1	1	1	0
Phe112	0	0	1	0	0	1	0	1	1	0	0	0	1	0	0	0	0	0	0	1	0	0	0
Phe74	0	0	0	1	0	0	1	0	0	0	0	0	1	0	0	0	1	1	0	1	0	0	0
Tyr72	0	0	1	1	0	0	1	1	0	0	0	0	1	0	1	0	1	0	0	1	0	1	1
Asp71	1	1	2	1	1	1	1	2	1	1	1	1	1	1	0	1	2	1	1	1	1	2	2
Met70[1]	1	2	1	1	1	2	1	2	2	2	2	2	1	3	0	2	1	2	1	1	1	1	1
Leu69[1]	1	2	1	1	1	1	1	1	1	1	1	1	1	1	2	1	1	1	1	1	1	1	1
Gly68[1]	0	1	0	0	0	1	0	1	1	1	1	0	0	1	2	1	1	1	1	2	1	2	2
Gly67[1]	0	0	0	0	0	0	0	0	0	1	1	0	0	0	1	1	1	0	1	1	2	1	1
Asn66[1]	0	0	0	0	0	0	0	0	0	1	1	0	0	0	1	1	1	0	0	0	1	1	0
Cys65	0	0	0	0	0	0	0	0	0	0	0	0	0	0	1	0	0	0	0	0	0	1	0
Glu63	0	0	0	0	0	0	0	0	0	0	0	0	0	0	1	0	0	0	0	0	0	1	1
Asn62	0	0	0	0	0	0	0	0	0	0	0	0	0	0	1	0	0	0	0	0	0	0	1
Gly61[1]	0	0	0	0	0	0	0	0	0	0	0	0	0	0	1	0	0	0	0	0	0	1	1
Trp26[1]	0	0	0	0	0	0	0	1	1	1	1	0	1	1	1	1	1	1	1	1	1	1	1
Cys25[1]	0	0	0	0	0	0	0	0	0	1	2	1	0	2	1	0	1	2	1	1	1	1	1
Ser24[1]	0	0	0	0	0	0	0	0	0	1	1	0	0	0	1	0	0	0	0	0	0	0	0
Gly23[1]	0	0	0	0	0	0	0	0	0	1	1	0	0	0	1	0	1	0	0	1	1	1	0
Cys22[1]	0	0	0	0	0	0	0	0	0	0	0	0	0	0	0	0	0	0	0	0	0	0	0
Gln21[1]	0	0	0	0	0	0	0	0	0	0	0	0	0	0	0	0	0	0	0	0	0	0	0
Gly20[1]	0	0	0	0	0	0	0	0	0	0	0	0	0	0	0	0	0	0	0	0	0	0	0
Gln19[1]	0	0	0	0	0	0	0	0	0	0	0	0	0	0	0	0	0	0	0	0	0	0	0
	1	2	3	4	5	6	7	8	9	10	11	12	13	14	15	16	17	18	19	20	21	22	23

Figure S6. Heatmap of flavonol/CatL interaction. Heatmaps are built on the logic of how many times each ligand interacts with each residue (regardless of bond type).

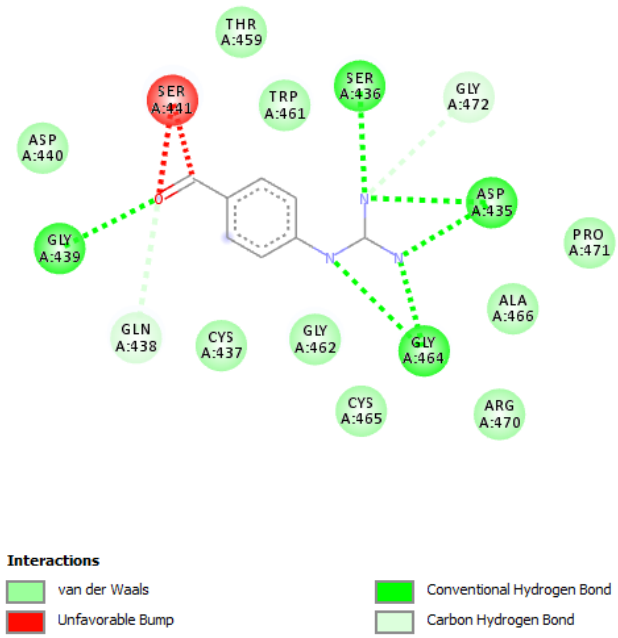

Figure S7. 2D interaction pattern of Nafamostat in the TMPRSS2-nafamostat complex (PDB ID: 7MEQ).